Physics – Uspekhi **65** (8) 812 – 833 (2022)

REVIEWS OF TOPICAL PROBLEMS PACS numbers: **42.25. – p**, 42.40.My, 42.50.Wk, **42.62. – b**, 42.62.Be, **42.79. – e**

Optical tweezers and manipulators. Modern concepts and future prospects

B V Sokolenko, N V Shostka, O S Karakchieva

DOI: https://doi.org/10.3367/UFNe.2022.02.039161

Contents

Abstract. The review aims to generalize fundamental concepts that are necessary for understanding the mechanisms and principles of optical trapping in both liquid media and air. One of the objectives of the article is to familiarize a wide audience with the global experience and the prospects for developing the fundamental principles of the functioning of optical tweezers for various purposes. The paper describes in detail the design options of optical manipulators in terms of versatility and energy efficiency of their use in a wide range of modern practical purposes and tasks.

Keywords: optical tweezers, optical manipulators, optical trap, gradient forces, photophoretic force, pulling force, structured optical fields

1. Introduction

In 1619 Johannes Kepler hypothesized that light can exert radiation pressure on irradiated objects. The hypothesis was based on observations of changes in the direction of a comet tail to the side away from the sun [1].

Theoretically, Maxwell predicted the existence of radiation pressure in 1873 based on the electromagnetic theory. To get new experimental proof of the validity of Maxwell's theory, it was important to measure the pressure of light. In 1891, the prominent Russian experimental physicist Petr Lebedev published the first, at that time purely theoretical, paper in the *Proceedings of the Department of Physical Sciences* of the Society for Natural Sciences devoted to repulsion forces acting on ray-emitting bodies. Almost ten years later, in 1900, P N Lebedev delivered a report at the World Congress of Physicists in Paris, which informed the scientific community about successful experiments on measuring the light pressure on solid bodies. In 1901, the results of experimental studies of momentum transfer from light to a thin foil suspended on an elastic filament in an evacuated vessel were published [2], which brought P N Lebedev worldwide recognition. General statements of the theory and specific features of the experiment, demonstrating the difficulties overcome by the researcher when measuring such small forces hidden among radiometric action and convection flows, have been illustrated by his pupils and followers [3–5]. In 1903, American physicists Nichols and Hull performed high-precision measurements of the momentum carried by light and confirmed the conclusion that the pressure of light depends only on its intensity and is independent of the wavelength [6].

In the 1950s, Russian physicists A V Gaponov-Grekhov and M A Miller investigated the localization of charged particles in inhomogeneous rapidly oscillating electric fields [7, 8]. The studies showed that, under the action of a high-frequency field, it becomes possible to create spatial traps that allow stabilizing the localization of the particles as well as their acceleration, independent of the electric charge sign. Note that the corresponding force, called the ponderomotive force or the high-frequency pressure force [9], depends on the intensity gradient of the light field. This fact directly relates it to gradient forces that take place in the theory of optical trapping and will be considered below.

With the invention of lasers, it became possible to use the forces of light pressure to capture and hold particles, which

B V Sokolenko (*), **N V Shostka** (**), **O S Karakchieva** (***)
V I Vernadsky Crimean Federal University,
prosp. Akademika Vernadskogo 4, 295007 Simferopol,
Republic of Crimea, Russian Federation
E-mail: (*)simplexx.87@gmail.com, (**)nataliya_shostka@mail.ru,
(***)olga.karakchieva@gmail.com

Received 21 May 2021, revised 19 October 2021
Uspekhi Fizicheskikh Nauk **192** (8) 867 – 892 (2022)
Translated by V L Derbov

led to the active development of new approaches to the noninvasive study of the properties of nano- and micro-objects. One of these approaches is based on the principle of controlling the spatial position of objects and their clusters through the interaction of laser radiation with matter in optical traps.

The method of optical trapping and the term 'optical trap' were first used by Arthur Ashkin [10] more than 50 years ago. Note that they are the light pressure forces on which the physical principle of trapping is grounded. Later, in 1986, another type of trap, the 'optical tweezer,' was presented based on gradient forces [11], which became a base for modern optical tools of trapping and manipulating transparent particles used in numerous biochemical, biophysical, physical, and engineering studies.

The growing interest in this method in recent years and the high appreciation of the significance of its basic principles are confirmed by the fact that in 2018 A Ashkin was awarded the Nobel Prize. It is worth noting that the subject matter is far from exhausted and the relevance of developing optical traps and improving optical manipulators based on them has only increased in recent years in connection with numerous practical studies, which became possible thanks to new scientific discoveries in this field. Notably, the technological perfection of modern optical and electronic devices has expanded the limits of application for previously developed methods.

The optical tweezer technique became most widespread in biological studies, since it allows one to hold and manipulate living cells in a medium close to natural for them. Note that, before the invention of optical tweezers, the study of biomolecular processes was restricted to bulk experiments, which yielded general averaged information about the cell population as a whole, groups of their elements, and molecules. The behavior of a single molecule remained hardly identifiable. The invention of optical tweezers made a revolution in biological and biophysical studies and offered the possibility of conducting hundreds of studies of single molecule behavior mechanisms, the micromechanical properties of these molecules, as well as forces and peculiarities of their interaction with other structural elements [12, 13]. For example, the basic mechanisms of myosin molecule operation, the basis of muscle contraction [14], the mechanical properties of DNA [15], as well as RNA-polymerase and biopolymer molecules [16] were explored. The interaction of neutrophils and pathogens was investigated. In Ref. [17], infrared optical tweezers were used to trap and manipulate erythrocytes inside murine subcutaneous capillaries in vivo. Quite recently, researchers managed to demonstrate optical tweezers of a new type, which made it possible to control the position of complex-shaped biological objects in all three dimensions [18]. Moreover, optical trapping and manipulation devices are promising in combination with optical tomography and digital holographic microscopy of biological objects. The implementation of three-dimensional trapping and keeping an object via optical fields of various configurations (structured fields, Hermite–Gaussian and Laguerre–Gaussian beams) [19–21] and full noncontact volume visualization offer substantially more possibilities than optical tweezers based on Gaussian beams focused with high-aperture lens elements.

It is important to pay attention to the fact that the use of optical trapping is becoming more and more relevant in such tasks as controlling and sorting microparticles in planar lab-on-a-chip structures [22, 23]. The integration of one-dimensional photonic crystals significantly extended the capabilities of these chips to trap particles, whose size is substantially smaller than the wavelength in the infrared range [24]. At the same time, so-called plasmon nanotweezers that use metallic nanoantennas to concentrate and enhance the incident radiation are easily integrated into such systems [25]. Such light-matter interaction forms intensity gradients in the near field, substantially enhancing optical forces at a given input power [26], thus ensuring stable optical trapping at the used radiation intensity 2–3 orders of magnitude lower than the threshold of the biological damage to the object [27].

The fundamental review article by a group of Russian scientists, V A Soifer, V V Kotlyar, and S N Khonina [28], presents in detail the physical principles of trapping and various experimental implementations of optical tweezers. At the same time, the considerable growth of effective approaches to forming beams applicable to trap nano- and microparticles under various conditions (*in vivo*, *in vitro*) makes it relevant to present an up-to-date scientific review, systemizing the existing solutions and trends of their development in application to the newest research problems. At present, the intense development of photonics is enhancing the relevance of systematization and generalization of the accumulated knowledge about the physical principles of the functioning of optical trapping devices. Stable trapping of micron and submicron particles is based on the optical properties of the matter composing these objects and their geometry, and, consequently, is determined by forces of interaction between particles and electromagnetic radiation. The principle, using the light pressure force acting on a transparent particle placed in an optical trap, became most widespread in designing 'optical tweezers' whose efficiency has been demonstrated by numerous achievements in this field in the five decades since their invention by A Ashkin.

2. Optical trap operation principle

The principle of operation of optical tweezers (optical traps) is based on the effect of focused laser radiation on nano- and micro-objects. Its main advantages are noninvasiveness (the absence of direct physical contact), the possibility of applying into a wide range of particles with different properties, configuration flexibility, the possibility of implementing various translations and manipulation in real time, and the choice of appropriate wavelength or optical trap properties — to provide nondestructive action of the trapped object [29, 30].

One of the parameters that determine the trapping efficiency is particle size. Optical traps are often used to contain objects ranging in size from hundreds of nanometers to tens of micrometers. Practical implementation of the stable trapping of nanoparticles smaller than the radiation wavelength remains a difficult problem, since optical trapping forces rapidly weaken with a decrease in particle size. Small-size particles are also inherently subject to thermal fluctuations and Brownian motion, which can destabilize the optical trap. To reduce the Brownian motion effect, it is possible to use, e.g., an environment with a higher dynamic viscosity coefficient. With increasing particle size, the gravity force grows too, which makes it necessary to increase the laser beam power and, therefore, the particle kinetic energy increases, at a certain value of which the trapping force becomes insufficient to hold the particle in the equilibrium position [31].

2.1 Classical optical trapping forces

A light wave can be considered a flow of photons, each carrying the momentum

$$p = \frac{h}{\lambda} = \frac{E}{c}\,, \tag{1}$$

where h is the Planck constant, λ is the light wavelength, and c is the speed of light in free space.

For a plane light wave incident normally on a surface, the light pressure is determined as

$$P = \frac{E(1+r)}{v}\,, \tag{2}$$

where r is the surface reflection coefficient, v is the speed of light in the medium, and E is the amount of incident energy per second.

Due to the interaction between the light wave and the object, a transfer of momentum from photons to the object occurs. The force acting on the object is caused by the change in the light momentum and is determined as the difference between momentum fluxes, corresponding to the absorption $\mathbf{S}_{\text{inc}}$ and reflection of photons $\mathbf{S}_{\text{refl}}$, given by the Umov–Poynting vector $\mathbf{S}$:

$$\mathbf{F} = \frac{n}{c}\int\!\!\int (\mathbf{S}_{\text{inc}} - \mathbf{S}_{\text{refl}})\,\mathrm{d}A\,, \tag{3}$$

where n is the refractive index, $\mathrm{d}A$ is an element of the irradiated area.

In the particular case of normal incidence of a plane light wave on an object surface, the optical force can be written in the following way:

$$F = n_{\text{env}}\frac{W}{c}\,Q\,, \tag{4}$$

where n_{env} is the refractive index of the environment, W is the total light power of the wave incident of the object, and Q is the coefficient depending on the parameters of the light wave and the particle to which the light force is applied.

In the case of 100% reflection of light by the object, the transferred momentum will be two times greater than given by Eqn (4), and in the case of oblique incidence, the force will be defined as $F\cos\alpha$, where α is the angle between the direction of the incident light beam and the wave vector after the interaction with the object.

The resultant of the forces involved in the optical trapping process and acting on the particle will be determined as a sum of two components: the gradient force F_{grad} and the scattering force F_{scat}. A force proportional to the intensity of the radiation and directed along the axis of propagation of the light beam is called the scattering force. The second, the gradient force, arises due to the presence of the intensity gradient (Fig. 1). In the case of a single-beam trap, the stable trapping of a particle is achieved via focusing by microscope objectives with high numerical aperture (NA $\sim$ 1.0), when the gradient force dominates the scattering one [32].

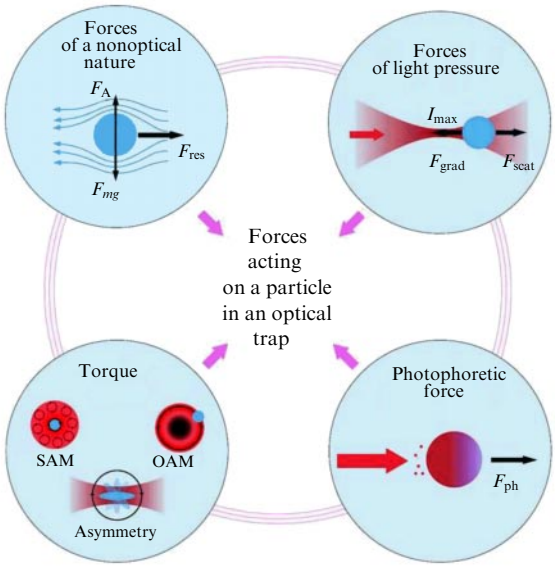

Figure 1. (Color online.) Schematic representation of the basic forces acting on an object optically trapped in its environment. By forces of a nonoptical nature, we understand the resistance force (prevails in a liquid medium), the gravity force (partially compensated by the Archimedean force in liquids; dominates in the gas medium), Brownian motion, thermal forces, and convection. OAM — orbital angular momentum, SAM — spin angular momentum, asymmetry — rotation due to the asymmetry of the particle shape.

Numerous analytical and numerical methods have been developed to calculate optical forces, the choice of which depends on the dimensions and shape of a particle, as well as on the optical radiation wavelength. When the size of the trapped particle is much smaller than the wavelength, the Rayleigh approximation method is used, and such a small particle can be considered a point dipole in a nonuniform electromagnetic field (Table 1) [33, 34].

For particles much larger than the wavelength, the trapping force is described using the ray optics model. In this case, the particle is considered a microsphere that deflects the rays from the initial direction because of the difference in the refractive indices between the particles and environment. The observed change in the momentum of both light and particles, due to the momentum conservation law, will lead to the appearance of a compensating force [34–36].

It is worth noting that most microparticles and biological objects used rigorously satisfy none of the conditions

Table 1. Approaches to the calculation of optical trapping forces.

Regimes	Subwavelength	Wavelength	Superwavelength
Approaches to the calculation of optical forces	Rayleigh approximation	Generalized Lorentz–Mie theory, T-matrix method, numerical methods	Geometrical optics
Size of particles	$r \leqslant 0.1\lambda$	$0.1\lambda \leqslant r \leqslant 10\lambda$	$r \geqslant 10\lambda$
Size of particles from the experimental point of view	$r \sim 10-250$ nm	$r \sim 0.25-10$ μm	10 μm $< r <$ 70 μm
Interaction with biological objects	Molecular level	Cell level	Integrated level

described above, since their size is approximately equal to the wavelength. To describe this case, the generalized Lorentz–Mie theory was initially used [37]. However, this theory is restricted to plane waves and objects having an ideal spherical shape. For real cases, the T-matrix method is used, which relates the incident field and the field scattered by a nonspherical object of arbitrary configuration [38].

More details about classical forces of optical trapping, as well as methods to calculate them, can be found in Refs [39–41].

Since optical beams with complex geometry, e.g., Laguerre–Gaussian beams, nondiffractive Bessel beams, and Airy beams, have come to practical use in optical manipulation, new types of optical forces acting on a trapped object have been investigated. They include the optical torque responsible for rotating a particle in an optical trap, the pulling force acting in the direction opposite to propagation of the optical beam, and the photophoretic force, which can be used to carry out optical trapping in the gaseous phase (see Fig. 1).

2.2 Rotational motion

From a practical point of view, an important role is played by the possibility of imparting rotational motion to a captured object. For example, in optically controlled sensors, rotary micromachines [42, 43], and the process of fine tuning of selective chemical interactions, controlled rotation is a fairly popular tool. Along with this, the angular orientation of trapped particles is used to study the properties of liquid and gaseous media, as well as the mechanisms of interaction among individual particles, living microorganisms, and molecules [44]. For example, in a high vacuum, symmetrical nanoparticles exhibit ultrafast rotation with frequencies up to 5 GHz [45], while maintaining an unprecedented sensitivity to environmental conditions. This approach has opened up new ways of studying a vacuum and its effect on the angular momentum of a rotating body [46], making it possible to study the friction mechanism associated with the interaction of solid matter and virtual particles of a 'quantum vacuum' [47].

The rotational motion of trapped particles can be caused by the action of structured light [48] or the simultaneous action of two parallel beams capturing an asymmetrically shaped particle [49–51] from opposite ends [52]. Simultaneous translation and rotation are implemented by changing the relative position of the traps [53] or the beam shape [54]. This gave rise to a unique technique of controlling the position and rotation of particles in a three-dimensional space using holders or optically controlled clamps [55, 56]. The relevance of using such tools is dictated by the necessity to reduce the degree of negative influence of light energy on living biological objects, their direct heating, and inducing photochemical reactions. Such micromanipulators and asymmetric particles can be oriented in a trap based on the holographic principle using a spatial light modulator [57]. Complex patterns of optical fields obtained in this way demonstrate two-dimensional rotation of extended particles by the example of *E. coli* [53] and a pair of coupled cells [58] within an angle range from 0° to 180° degrees in the (y, z) plane, studied using tomographic phase microscopy.

As an alternative to using structured optical beams, there are other methods of optical rotation of objects, e.g., at the expense of shape asymmetry of the particle itself. In this case, the torque arises due to the nonuniform scattering or absorption of light [59, 60]. It should be taken into account that, the smaller the particle, the weaker the dependence on its geometry.

There are several types of object rotation in an optical beam: rotation about its own axis, rotation along an orbit around the beam axis, and two-dimensional tilts [61]. An optical trap based on counterpropagating laser beams allows a rotational motion of the captured particles if the beams are slightly noncoaxial [49, 62], which is easy to implement using optical fibers [63]. The magnitude of the gradient and scattering forces, their spatial distribution, and, consequently, the geometry of the circular trajectory and the rotation velocity are controlled by changing the distance between the fibers, the displacement of the core from a given axis, and the beam power.

A fundamentally different case of imparting rotation to a trapped particle can be realized by transferring light angular momentum, which can be represented as the sum of the projections of the orbital angular momentum L_z and spin angular momentum S_z onto the propagation axis (see Fig. 1). For a paraxial singular beam in free space, the projection of the angular momentum can be written in the following simplified form: $\Omega_z = L_z + S_z$.

The orbital angular momentum is often understood as the flux density of the angular momentum of the electromagnetic field wave in a beam. Beams with wavefront singularities carrying orbital angular momentum were first mentioned in the article by J Nye and M Berry [64], where a detailed analysis of the field states with a helicoidal wavefront was presented. In addition to the orbital angular momentum, a polarized optical beam can carry a spin angular momentum due to the presence of circular polarization. For example, for a linearly polarized beam, the spin angular momentum will be zero, and for a circularly polarized beam, it will be $\pm\hbar$, where $\hbar$ is the reduced Planck constant. The choice of sign depends on the direction of circular polarization, as proposed by Sadovsky in 1899 and Poynting in 1909 [65].

The transfer of the light beam spin angular momentum and its conversion into a mechanical one were first demonstrated in the experiment by R Beth in 1936, in which the torque imparted to a half-wave plate suspended in air was measured [66]. Therefore, for efficient transfer of the angular momentum from a beam with circular polarization, the particle should contribute a phase delay multiple of an odd number of π. It follows that the thickness of an anisotropic particle will be a decisive parameter.

Particularly, in a linearly polarized beam, an anisotropic particle can also be made to rotate, since it tends to orient along the polarization vector. Among examples of such particles, we can mention silicon dumbbell [67] and cylindrical [68] nanoparticles, diamond crystals [69], etc. [70, 71]. Under the polarization rotation, the particles follow the direction of the electric field strength vector and turn around their own axis. When the light polarization is switched from linear to elliptical, the trapped particle undergoes continuous rotation, the angular velocity of which depends on the fraction of circular polarization [72] in the beam field. For example, in the process of transformation of an anisotropic particle of circular polarization of light into a linear one, a torque on the particle will be optically induced due to the law of momentum conservation. The angular velocity of the particle will be determined by the optical torque produced by the laser beam and the viscous resistance of the environment acting on the particle.

The presence of singularity in the wavefront structure, e.g., slanting or screw-shaped surfaces, in which the wave vector direction does not coincide with the beam propagation

axis, can cause a rotational motion of particles along a closed trajectory due to the presence of orbital angular momentum [73]. To acquire rotational motion, a particle should be irradiated with a beam carrying an optical vortex, and the most widespread analytical solution to describe such fields belongs to the family of Laguerre–Gaussian modes [74]. The azimuthal number (l) of a Laguerre polynomial determines the orbital angular momentum $\pm l\hbar$ per photon. The number l is also known as the 'topological charge' and takes positive and negative values. The chosen sign determines the sense of the trapped particle rotation.

The transverse intensity profile of Laguerre–Gaussian beams has the shape of a ring of maximum intensity with a central minimum, the diameters of which depend on the topological charge. Particles whose linear dimensions are larger than the diameter of the vortex beam can be trapped at its center and demonstrate circular motion about their own symmetry axis [75], and particles of smaller size acquire a characteristic rotation along a circular trajectory inside the intensity minimum (for strongly absorbing particles) or along the intensity maximum (for transparent ones) [76, 77]. An important feature of such beams is that the topological charge magnitude predetermines the motion dynamics [78] and allows controlling the rotation velocity or performing indirect measurements by characterizing the particle response to the parameters of the environment [79]. Note that asymmetric objects can rotate in both scalar and vector fields [80].

Reference [81] experimentally studied the dependence of some aspect of particle motion in an optical trap on different contributions from the spin and orbital angular momenta of the light beam. It was found that the effect of the spin angular momentum leads to particle rotation about its own center, while the orbital angular momentum, in turn, causes particle rotation around the beam axis [82–84].

It is known that, even possessing no birefringence, spherical objects can be made to rotate by transferring orbital angular momentum in the processes of absorbing and scattering part of the light energy [85]. The greater the absorption capacity, the higher the achievable efficiency of torque transfer from a circularly polarized beam.

Note that, in anisotropic media and in a nonparaxial beam, whose waist radius is comparable to the wavelength, the contributions from spin and orbital angular momenta cannot be separated [86], accounting for the practical importance of considering the total contribution to the rotational motion of particles [49]. For example, the efficiency of transfer of the orbital and spin angular momenta will be determined by the absorption or scattering index of the particle surface, as a result of which transparent microspheres manifesting no anisotropic properties demonstrate a rotation upon their exposure to an optical vortex [76]. The interrelation of spin and orbital angular momenta is complicated in strongly focused beams whose waist radius is comparable to the wavelength, due to which spin-orbit coupling arises, manifesting itself in the character of the rotation of the trapped particles [87].

An important feature of the interaction of light carrying angular momentum and trapped particles is its manifestation on the subwavelength scale, in particular, in plasmonic nanotraps [88] and in traps formed by surface waves near nanofibers [89]. Controlling the rotation dynamics of trapped polystyrene scattering microspheres in such an optical system is ensured by travelling and standing evanescent waves excited by counterpropagating beams with elliptic polarization.

2.3 Photophoretic forces

Until recently, implementing the stable trapping of light-absorbing particles in the gaseous phase remained an open question. In most optical traps, the capturing forces are the forces of light pressure, which are rather weak. The situation is substantially complicated because of the effect of the gravity force, which is mostly comparable to or exceeds the light pressure forces. Therefore, efficient trapping by light pressure forces was initially executed in liquid media, where the effect of gravity is not so significant, or in vertical traps used in experiments on optical levitation, where the scattering force, induced by a focused laser beam, balances the gravity force.

At present, for trapping light-absorbing particles suspended in a gaseous medium, the photophoretic force is used as an alternative to and more efficient mechanism than radiation forces. For absorbing particles, this force exceeds the radiation forces by a few orders of magnitude [90, 91]. A feature of the formation of photophoretic optical traps [92] is the use of 'hollow beams,' e.g., Bessel–Gaussian beams [93], whose energy scattering and the degree of diffraction by particles make it possible to provide a more stable trapping [94] than beams with a Gaussian envelope [95] used to control the position of particles of an asymmetric extended shape, for example, *E. coli*.

The mechanism responsible for the appearance of such forces is the following: when irradiating a particle in an optically transparent environment, the particle absorbs virtually all the wave energy, increasing the mean kinetic energy of molecules in the absorbing regions. Consequently, the momentum transferred to gas molecules increases, and zones with nonuniformly distributed pressure in the environment and with a nonuniform distribution of temperature on the surface of the irradiated particle appear. The particle will move towards the zone of minimum pressure; therefore, beams with a minimum of intensity on the axis are used for trapping by a photophoretic force. A particle that finds itself in the near-axial region of such a beam cannot penetrate through the light walls. Any displacement of the particle leads to heating of its part which is nearer to the zone of maximum intensity and farther from the beam center. The arising pressure difference between the less heated center and the periphery with higher surface temperature returns the particle into the position of stable equilibrium at the beam axis.

Earlier, photophoretic forces were considered only in the case of trapping in air, and they were commonly ignored when trapping in liquids. Nevertheless, in Ref. [90], the trapping by photophoretic forces in a Bessel beam was demonstrated in a glycerol solution.

In an ideal case of irradiating a spherical thermally homogeneous particle with a plane wave, the photophoresis force can be presented in the following form:

$$F_{\mathrm{ph}} = -J_1 \frac{9\pi\mu_{\mathrm{env}}^2 r_{\mathrm{p}} I}{2\rho_{\mathrm{env}} T(k_{\mathrm{p}} + 2k_{\mathrm{env}})}\,, \tag{5}$$

where μ_{env} is the environment viscosity, T is the air temperature, I is the intensity of the incident beam, r_{p} determines the particle size, k_{env} and k_{p} are the heat conduction coefficients of the environment and the particle, respectively, and parameter J_1 depends on the particle absorption coefficient and determines the distribution of the absorbed energy over the particle volume. For example, for a particle completely absorbing the radiation, $J_1 = 1/2$.

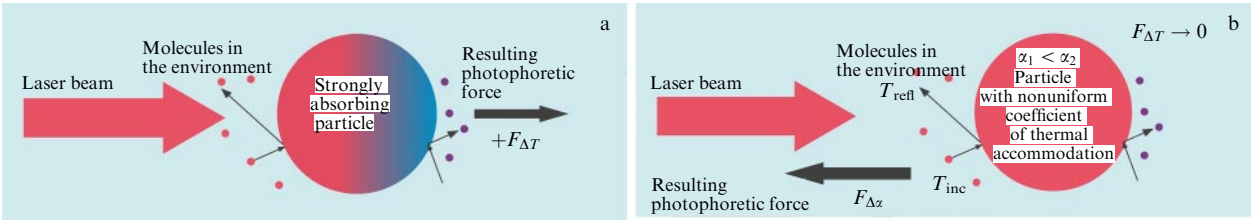

Figure 2. (Color online.) Example of trapping by ΔT-type (a) and $\Delta\alpha$-type (b) photophoretic forces.

Calculating the photophoretic force for arbitrary particles with indefinite properties, e.g., size, shape, and heat conductivity, is still a difficult problem that requires solving the electrodynamics equations. The magnitude and direction of the photophoretic force will directly depend on the physical parameters of the particle, such as density, heat conductivity, absorption ability, and the geometry of the particle, as well as the thermal properties of the environment.

In optical trapping by thermal forces, it is accepted to consider two types of photophoretic forces, one of them, $F_{\Delta T}$, arising due to the temperature gradient and the other one, $F_{\Delta\alpha}$, being a result of a change in the thermal accommodation coefficient α and determined by the coefficient of heat exchange between the particle and the environment [96–98]. Let us write the accommodation coefficient as $\alpha = (T_{\text{incg}} - T_{\text{reflg}})/(T_{\text{p}} - T_{\text{reflg}})$, where T_{incg}, T_{reflg} are the temperatures of gas molecules incident on and reflected from the particle surface, and T_{p} is the temperature of the particle surface.

The force $F_{\Delta T}$ can have both positive and negative direction relative to the optical beam propagation, depending on the temperature difference on the surface of the trapped object (Fig. 2a). That being said, $F_{\Delta\alpha}$ is independent of the temperature distribution on the object surface and is determined by its geometry. One of important properties of this component is its ability to impart rotational motion to the trapped particle. Upon uniform heating of the particle surface ($F_{\Delta T} \to 0$), $F_{\Delta\alpha}$ begins to dominate the component $F_{\Delta T}$, since $F_{\Delta\alpha}$ is induced by the difference in rates of heat exchange between the environment and individual fragments of the particle surface and is directed from higher to lower values of the accommodation coefficient (Fig. 2b) [90, 99]:

$$F_{\Delta\alpha} = \frac{\pi\eta^2\sigma J_1 I^2}{12\rho k_{\text{env}} T k_{\text{p}} (\bar{T}_{\text{p}} - T_{\text{env}})}\,. \tag{6}$$

Here, σ is the particle cross section, I is the intensity of the incident beam, ρ is the viscosity coefficient, T_{env} is the temperature of the environment molecules hitting the particle surface, and $\bar{T}_{\text{p}}$ is the averaged temperature of the particle surface.

2.4 Pulling force

In recent years, a force whose direction is opposite to the light wave propagation has attracted much attention of researchers because of its unique capability to transport particles optically over a relatively large distance compared to classical traps. This force is called the 'pulling force' or 'force of negative radiative pressure' [31].

Generally, the momentum imparted to the object is greater than that of the scattered photons, due to which, according to the momentum conservation law and the Newton's second law, the force acting in the direction of light propagation arises. Therefore, for the appearance of the pulling force directed oppositely, it is necessary to

— either increase the momentum of the scattered photons with respect to the momenta of the incident ones

— or decrease the momentum of photons incident on the object with respect to the scattered ones, because of which the particle affected by the arising force will move oppositely to the electromagnetic wave propagation, i.e., towards the radiation source [99], because of certain combinations of the parameters of the light wave, trapped object, and environment [100].

The mechanisms of the pulling force formation are often divided into four kinds [101, 102].

— *Using structured light or interference of laser beams* [100, 103–105]. For example, it was shown that, using a set of slanted plane waves or the interference of two Gaussian beams [100], it is possible to reduce the input momentum, the forward scattering by the object being maximum. The main criterion for the appearance of the pulling force in this case is a large angle of $\sim 170^\circ$ between the two incident beams, which facilitates the forward scattering. The pattern of the scattered field is closely related to the polarization of the incident light, and the light intensity distribution is not the main criterion for the force's appearance. Beams with identical patterns of intensity distribution give rise to qualitatively different dependences of the formation of the pulling force due to differences in their vector (polarization) structure [106].

In Refs [107–109], it was proposed to use Bessel beams, which can be considered a superposition of plane waves, whose wave vectors form a cone with the vertex angle α with respect to the axis of beam propagation. In this case, the force of negative radiation pressure is subject to some limitations: for Rayleigh particles, it vanishes, because, in this case, the interference effects can be ignored due to the limited size. The second factor affecting the origin of pulling forces is the cone angle of the Bessel beam: at values $\alpha > 60^\circ$, the arising force does not depend on the material or size of the particle [105].

— *Using a structured environment*. The environment can serve as a substantial element in the implementation of particle motion in the opposite direction. There are numerous methods for modifying the properties of the environment to create a back flux of particles. For example, the environment can be modified at the expense of the negative refractive index, which gives rise to the force of negative radiative pressure [110, 111].

— *Varying optical parameters of the trapped objects* [112]. For example, cylindrically shaped dielectric particles, like other kinds of elongated objects such as optically coupled particles, are used to create and enhance the pulling force [113]. Reference [108] demonstrates the movement of trapped particles towards the radiation source, the particles being microspheres and cylinders possessing optical gain. This

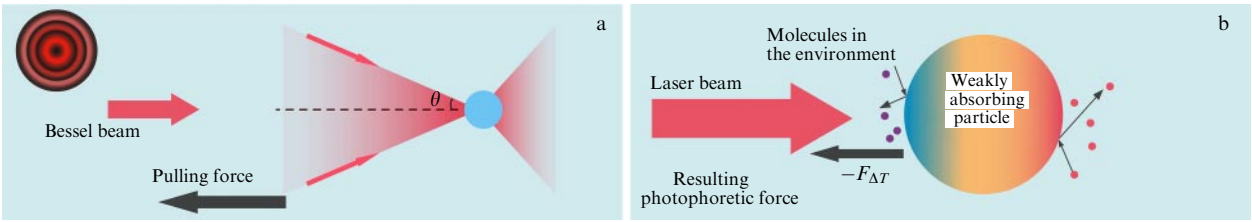

Figure 3. (Color online.) Illustration of the mechanism forming an attraction force, directed opposite to the light flux, via the example of a Bessel beam (a) and due to a photophoretic force (b).

approach allows increasing the momentum of the emitted photons in comparison with the incident ones due to stimulated emission.

— *Formation of a negative photophoretic force* [114]. Weakly absorbing spherical particles act as lenses and focus light on the dark side of their surface, due to which that side acquires a higher temperature than the opposite irradiated side. Because of this fact, the effect of negative photophoresis is observed (Fig. 3b). For example, the authors of Ref. [115] have experimentally shown that, in the case of trapping hollow glass spheres with a gold nanolayer sputter coating by cylindrical beams in the air, a negative optical force appears, depending on the beam polarization. For a radially polarized beam, the trapped semitransparent microsphere moves in the direction of beam propagation, while, for an azimuthally polarized beam, the motion occurs in the opposite direction, towards the radiation source.

Methods for calculating the pulling force are similar to those for calculating classical forces of optical trapping [116]. The reader can find more details about pulling force mechanisms in reviews [101, 117].

3. Classification of modern optical systems for trapping and manipulating micro- and nanoparticles

The stability of trapping micron and submicron particles is based on the integrity of a number of factors, such as the optical properties of the matter composing the particles and their geometry and, consequently, is determined by the forces of the interaction of the particles with electromagnetic radiation. The principle of using light pressure forces acting on a transparent optically trapped particle has found most application in the design of 'optical tweezers,' the efficiency of which has been demonstrated by a variety of achievements in this field in the five decades since their invention by A Ashkin.

A combination of simplicity and functionality in optical tweezers requires the fulfilment of the basic principle — the gradient force must dominate the scattering force, particularly for particles having positive polarizability (the refractive index of the particle is greater than that of the environment) [118]. For this purpose, a Gaussian beam is focused using objective lenses with high numerical apertures (frequently, NA > 0.95), making it possible to form a considerable gradient of the light field intensity near the focus.

To achieve stable trapping, particularly of massive and large-size particles, counterpropagating beams are used. The combined action of oppositely directed scattering forces in such a trap compensates for their contribution; the counterpropagating beams can be formed separately, as well as by reflection of the initial trapping beam from a parabolic mirror placed behind the microscope objective focus [119].

Applying the principle of equilibrium of forces acting on particles in an optical beam has allowed considerable improvement of the technological principles of and design solutions for optical traps in recent years, among which the following can be conditionally distinguished: single-, double-, and multiple-beam traps; traps based on evanescent waves; and contact manipulators, controlled by optical beams (Fig. 4). Such a variety of optical trap configurations is due to a variety of trapped objects differing in their natures: transparent and absorbing (reflecting), optically more or less dense in comparison with the environment, and with spatial dimensions from a few nanometers to hundreds of micrometers.

This section is devoted to the classification of modern optical traps, aimed at demonstrating the basic operation principles of optical schemes, their main capabilities, and their limitations.

3.1 Single-beam traps

In 1987, A Ashkin et al. [36] presented an optical trap (known as 'optical tweezers') using a single Gaussian beam focused with a microscope objective with a large numerical aperture [120]. In such a trap, the condition of particle trapping stability holds if the ratio of the gradient force to the scattering force is greater than one, which corresponds to a region of maximum gradient of the field intensity. The axial position of the trapped particle in this case can be determined by the relation $z = \pi\omega_0^2/\sqrt{3}\lambda$; here, the particle will tend to the equilibrium position near the focus (Fig. 4a).

Single-beam traps are constructively based on the 'inverted microscope' optical scheme, in which the objective is placed below the preparation with particles and the beam is directed from bottom to top, providing their 'optical levitation.' Such a solution allows partial compensation for the scattering force by the gravity force and increasing the axial stability of trapping even in beams weakly focused by lenses with a numerical aperture that is not large [121].

The use of a single-beam trap using gradient forces made it possible to provide a full three-dimensional trapping of particles even with insignificant laser radiation power of a few milli-watts, hitting the region of particle trapping [122]. Along with this, a principal limitation of this configuration is the difficulty controlling the trapped particle position, implemented mainly by passive mechanical displacement of the objective lens, lenses of a 4*f*-optical system, or the preparation itself.

The single-beam trap principle was further developed just from the point of view of precise control of the trapping region position by means of various electronic and acoustic modulators.

Using an acousto-optic deflector, several positions of the optical trap are scanned; the frequency of visiting trapped

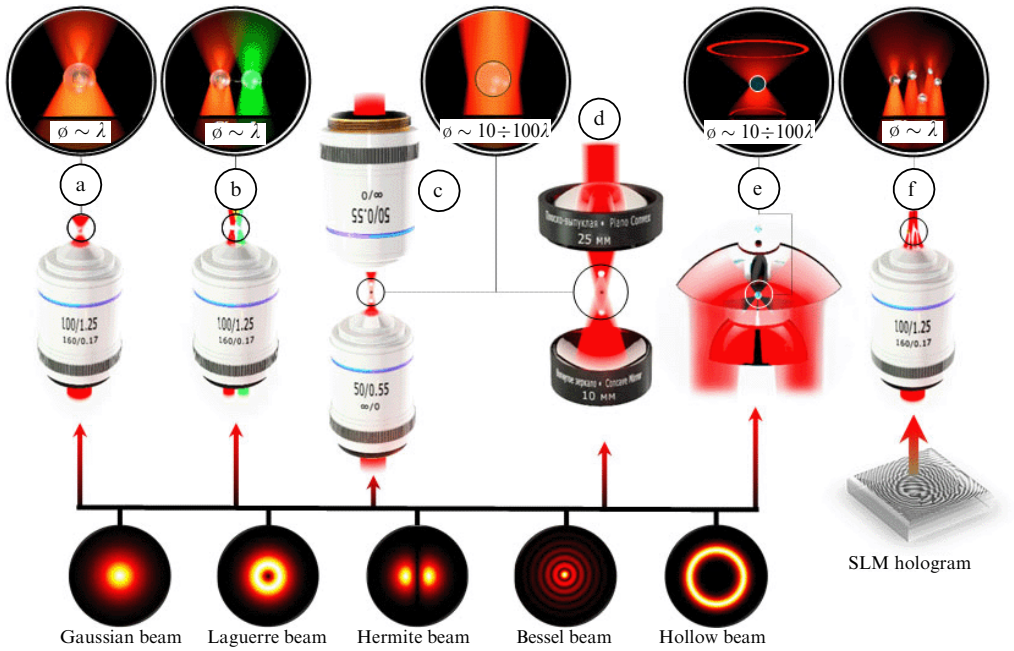

Figure 4. Schematic representation of optical trapping systems based on discrete elements: optical tweezers (a); double-beam traps (b–e); multi-beam trap using a spatial light modulator (f). Typical dimensions of trapped particles are indicated in the figure; λ is the radiation wavelength.

particles should be from 1 to 10 ms to prevent their release [121]. One of the solutions to the problem of creating dynamic optical traps was implemented by sequential scanning of a given number of positions by a laser beam reflected from galvanometric scanner mirrors and forming a time-averaged spatial pattern of light in optical tweezers [123, 124].

The use of electronically controlled liquid crystal cells [125] and spatial light modulators allowed creating active completely three-dimensional manipulator traps with a submicron accuracy in positioning the trapped particles. Russian scientists from Korolev Samara National Research University have demonstrated an efficient method of generating dynamically tunable single-beam traps. It is based on diffractive optical elements (DOEs) and holograms, reproducible using optical modulators. Advantages of DOEs fabricated using the substrate etching technique [126] and optical lithography include resistance to high-power laser radiation, a relatively high diffraction efficiency of beam conversion (22% or more) [127], and the possibility of generating a variety of beams: Bessel [128–130], Laguerre–Gaussian [78, 131, 132], Hermite [133, 134], Airy [131, 135], hollow [128, 136, 137] and bottle-shaped [138, 139]. Optical traps with the above beams and their combinations formed using DOEs and optical modulators opened the possibility of dynamic selective trapping and manipulating transparent and absorbing particles both in liquid and in gaseous (air) environments by single-beam optical traps [140, 141]. One of the examples of using such traps is the construction of a volume holographic display, in which the trapped particle plays the role of a voxel and can move at a speed of 1827 mm s^{-1} in air [124].

As a means of miniaturizing and extending the functional capabilities of single-beam traps, optical fibers are widely used (Fig. 5a), by which three-dimensional trapping was first demonstrated in 2006 [142]. The stable trapping of a particle in the longitudinal direction was implemented by means of a lens-like end face; the trapping region in this case is localized between the foci of the modes [143].

Optical fibers of a complex structure, for example, with several cores, make it possible to control the position of trapped particles with five degrees of freedom. To achieve greater values of the gradient force, the fiber end faces are modified by attaching spherical microlenses and lenses with a refractive index gradient, total reflection prisms, that are needle-like in shape [144], thus increasing the fiber numerical aperture. For this purpose, the three most widespread methods used are etching the end with hydrofluoric acid, drawing the heated fiber, and ion or two-photon lithography. The core of an optical fiber with an axicon at the end [145–147] allowed producing a Bessel beam and opened the possibility of simultaneous trapping multiple particles in the axial region of the field, substantially less subjected to diffraction. To prevent the trapped particle from touching the optical fiber surface,

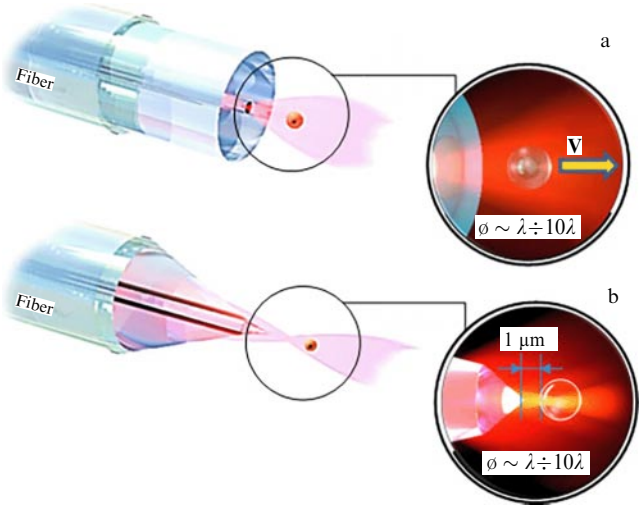

Figure 5. Schematic representation of fiber optical manipulators: 'pushing' two-dimensional manipulator (a); three-dimensional optical trap based on light pressure forces (b) [148]. Typical dimensions of trapped particles are indicated in the figure; λ is the radiation wavelength.

the authors of Ref. [148] proposed an experimental method of two-stage etching of the fiber up to the formation of the cone angle at the end close to 90° (Fig. 5b). The effect of self-focusing in fibers with a refractive index gradient and lens-like end face has also been exploited for optical trapping. In this case, the focus axial position is controlled using an air gap between the fragments of a single-mode fiber and a fiber with a gradient refractive index [149].

The implementation of a flexibly controlled system of optical tweezers using optical fibers is described in a number of reviews [120, 150, 151] and original papers [152]. Combining waveguides with evanescent-wave and plasmon-polariton optics [153] based on nanostructured resonators opens up a number of promising solutions for creating tools for non-invasive manipulation of nanostructures [154, 155], individual cell organelles, in particular, DNA nucleotides, whose dimensions are units and tens of nanometers [156].

One of the approaches to increasing the efficiency of single-beam traps in recent years is to search for solutions to overcome the focusing diffraction limit. One method is to use the so-called 'photonic nanojet' arising when a beam is focused by a spherical or cylindrical microparticle from 2 to 6 μm in diameter [157]. In this case, the half-width of the photonic jet focal spot can be $< 0.4\lambda$ for a particle refractive index close to two [158, 159].

The simplest system of optical trapping by gradient forces arising in a photonic nanojet consists of an optical fiber, to the end of which a polystyrene microsphere is electrostatically attached [159]. The advantage of such a configuration is the improved sensitivity to signals of fluorescence and back-scattering due to the increase in the numerical aperture, which has given a significant boost to the applied aspect of using optical trapping in combination with fluorescence and Raman microscopy *in situ* [160]. Later on, this effect was used as a basis of interaction of *E. coli* joined in a long chain [161] so that each following bacterium was attached to the free end of the previous one that played for it the role of somewhat of a waveguide and a gradient force source [162]. The result of such clustering of cells, e.g., red blood cells, is called a 'cellular waveguide' [163].

3.2 Double-beam traps

Historically, the first optical trap presented by A Ashkin in 1970 [10] had two counterpropagating focused coaxial beams, in the overlap region of which the stable trapping of a glass microsphere occurred on the axis, mainly due to the scattering forces in an aqueous medium and gradient forces acting in the radial direction (Fig. 4c) [121]. Such a double-beam trap has a high degree of trapping stability due to the compensation of longitudinal translation of particles by scattering forces of each of the counterpropagating beams, as well as flexibility in controlling the optomechanical systems, which allowed using this scheme to capture particles in the air [164, 165] using no microscope objectives with a high numerical aperture. However, the counterpropagating beams and the overlap region should be rigorously coaxial and symmetric; otherwise, due to even a small imbalance of forces, the character of particle motion becomes complex. In this case, the particle begins to move toward the beam with smaller optical power until a new equilibrium position appears [120, 166, 167].

A double-beam trap is usually formed by two independent beams obtained using beam splitting optics, which requires precise positioning of the beams in the (x, y)-plane, but, in turn, complicates the optical scheme and alignment procedure [168]. This requirement is particularly relevant for traps that allow transporting particles over distances significantly exceeding the particle size, up to a few ten centimeters [165].

In 2016, C Wang et al. [164, 169] demonstrated levitation and control of the axial position of carbon nanotubes 5 nm in diameter and 10–30 μm long in an air environment using a double-beam trap. The optical trap in Wang's scheme was formed by a beam from an argon laser with a power of 500–1000 mW focused with a lens with a focal length of 25.4 mm. The counter beam was formed by reflection from a concave mirror with a focal length of 10 mm (Fig. 4d). Such a solution allowed essential simplification of the trap design, improving its reliability and the precision of particle positioning. Moreover, the range of axial particle displacement was limited by the depth of controlled overlap of the beams and was from 20 to 100 μm, which also provided a possibility of trapping an ensemble of a few particles. Later on, A Kalume [170, 171] demonstrated the control of the axial position of liquid microscopic droplets with a diameter of 20–25 μm in air using a similar scheme and hollow beams [168].

Double-beam optical trap setups became widely used for problems concerning the capture of light-absorbing particles in free space (air and vacuum) [119, 172]. In contrast to single-beam traps based on gradient forces, they allowed creating conditions for trapping by scattering forces and mainly by the photophoretic force [169, 173]. However, this approach is demanding on the profile of the light beams providing capture. Besides Gaussian beams, Laguerre–Gaussian beams, also known as vortex beams, are used to form double-beam traps [78, 174, 175]. When superimposing the beam cones (Fig. 4e), a region of intensity forms in their overlapping zone, whose spatial profile resembles a bottleneck with a minimum on the axis. The particle captured by such a trap can move along the beam axis within the limits of the distance between two foci, the motion amplitude being a few millimeters [121].

Along with Laguerre–Gaussian beams, Bessel beams are used in the practice of double-beam optical trapping [128, 176, 177]. Due to the diffraction-free property within the focusing depth, transparent and absorbing particles localize, respectively, in the regions of maximum and minimum intensity of the light rings. The family of optical elements offers a wide choice of methods for the formation of Bessel beams using axicons [129, 147], DOEs [121, 178], and holograms [179], also applicable for producing so-called tubular or 'hollow' beams based on a superposition of Bessel beams [140].

As a particular case of a double-beam trap, we can consider a gradient trap formed by a microscope objective with a large numerical aperture, similar to a single-beam trap. In contrast to the latter, the scheme uses two independent beams focused by one common microscope objective (Fig. 4b) [170, 180]. The flexibility of this method of organizing a trap allows using coherent and incoherent beams. As a result, the trapping of particles with a refractive index greater or smaller than that of the environment can be performed in the interference field produced by coaxial coherent beams [181], as well as independently in the focal region of each of them. This approach is widely used in studies of intercellular and intracellular interaction *in situ* [182–184] to characterize the molecules of DNA and proteins [185, 186] in measurements of thermodynamic parameters and forces [187].

All the advantages of double-beam traps based on counterpropagating beams are inherent in optical fiber systems. Constable et al. [188] first proposed this solution in 1993. The diverging beams emitted by two fragments of

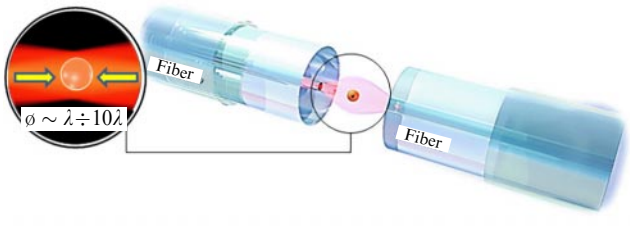

Figure 6. Design of a double-beam optical trap based on counterpropagating beams emitted by optical fibers. Trap ensures three-dimensional capture and positioning of particles with sizes $\lambda \div 10\lambda$, where λ is the wavelength of radiation.

oppositely directed single-mode fibers form an optical trap in the region of standing waves, where the scattering forces compensate for the action of each other, the particle being held on the beam axis by the radially directed weaker gradient force (Fig. 6).

Promising results of optical trapping of a large number of cells by double-beam fiber traps have been demonstrated in Ref. [143]. The so-called 'optical binding' of transparent particles with a symmetric surface shape and positive polarizability (*E. coli*, red blood cells, microspheres) is produced by weakly focused optical beams formed by the needle-like ends of the fibers. Because of the considerable prevalence of the cross section of the beam fields radiated by the fibers over the particle sizes, stable trapping in such a system can be achieved simultaneously for an ensemble of a large number of microobjects. The optical binding mechanism is similar to the action of a photonic nanojet, formed by the cell structures themselves, joined into chains [189] held to each other by locally increased gradient forces in the neighborhood of the jet. Such forces are called 'binding forces' in the world literature [190, 191].

The focal length and, consequently, the position of particles in fiber traps can be controlled by changing the coaxiality of the fibers and the distance between them (for the case of counter-fiber manipulators), which makes the particle move towards the end that emits less power, simultaneously undergoing rotation.

The advantage of using optical fibers to design double-beam traps consists in miniaturization and the possibility of their integration into microscopy and lab-on-a-chip systems, as well as direct introduction into the object of study.

3.3 Multi-beam traps

The possibility of simultaneous trapping of an ensemble of a few particles using single- and double-beam traps has been demonstrated in many papers, beginning with the very first experiments in the field. Significant discoveries over the last one or two decades in the field of medical and biological studies, microrobotization [56, 192], and materials science [141] have been achieved due to the possibility of targeted and simultaneous control of each of the particles captured in an optical trap.

The first attempts at spatial structuring of a large number of particles (to a few tens and hundreds) into an array with the specified configuration were based on the interference of several, e.g., three and five, beams [193, 194] obtained by amplitude or wavefront division [195] and producing a quasiperiodic field pattern in the region of their superposition. Such an approach allowed improving the mechanisms of sorting particles of different sizes at the expense of changing the shape and position of the 'optical lattice' [196, 197]. To reduce the number of optical elements and to increase the resistance to mechanical perturbations, this method acquired a new development twist by using various diffraction gratings and amplitude masks. It is worth noting that such an approach is still used with regard to problems controlling the relative position of both absorbing and optically transparent particles in a certain volume of a liquid or gas [198, 199]. At the same time, even when having achieved a specified spatial distribution of the entire ensemble, it is impossible to move individually chosen particles from one spatial point to another without destroying the general arrangement. The solution that allowed avoiding this difficulty was to use the holography method.

The holographic principle of light field formation as a tool for optical trapping and manipulation was first proposed in 1998 using a liquid-crystal spatial light modulator (SLM) placed in the way of a laser beam (Fig. 4f) [200]. Based on this approach, one can divide one incident coherent beam into several independent beams using holograms, whose structural organization is dynamic and forms in real time [201, 202].

For full-value three-dimensional trapping of particles, individual beams in the plane of the trap are formed by reflecting or transmitting SLMs placed in the conjugate focal plane of a microscope objective, which is achieved using a 4*f*-system of lenses. Such an optical multibeam trap is called 'holographic optical tweezers' and is currently widespread in many applied studies of biological systems and atmospheric phenomena, e.g., controlling the position of aerosols and microdroplets of a liquid with their organization into arrays of arbitrary shape [203]. As an alternative to SLMs, binary digital micromirror devices (DMDs) are being considered, characterized by efficacy of operation in a wide range of wavelengths and with high density of radiation energy [204].

There are several algorithms to calculate digital holograms and perform their subsequent encoding on a modulator with the purpose of creating multibeam traps, including vector beams [205]. Among them, the two most widespread methods stand out, namely, the Gerchberg–Saxton algorithm [206] and the algorithm of numerical modeling prisms and lenses [207]. The choice of an appropriate algorithm depends on the conditions of the experiment from the point of view of the efficiency of converting laser beam energy, the accuracy of trap positioning in two- and three-dimensional space, and the computing speed [208].

For example, Padgett et al. [209] proposed and made publicly available an algorithm, 'Red Tweezers,' for holographic optical tweezers based on calculating the fields of individual traps and their superposition.

3.4 Traps based on evanescent waves

The optical trap capability to hold a particle in a restricted region of the trapping beam field is based on a number of conditions, such as the contrast in refractive indices between the particles and the environment, the absorption coefficient at the specified wavelength of the trap, and the ratio of particle mass to size. The last parameter becomes a key one when choosing the trapping optical scheme, since the particle size determines the beam focusing conditions and radiation power.

Trapping particles whose cross section is of the order of a tenth of the wavelength, up to a few nanometers, is today the most interesting and at the same time the most difficult task. It is known that the gradient force magnitude cubically depends on the transverse dimension ($\sim r^3$) of the trapped

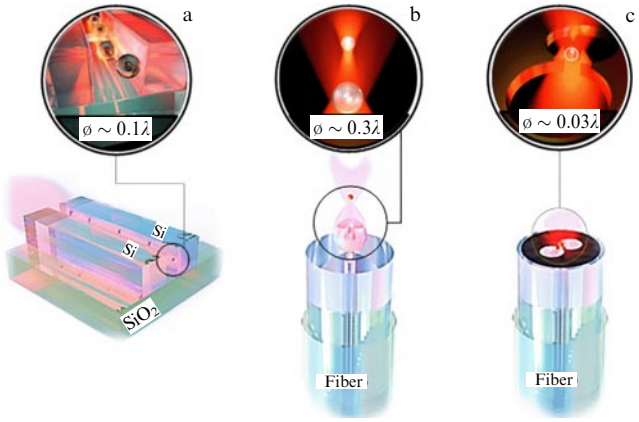

Figure 7. (a) Slit waveguide formed by two parallel planar silicon optical fibers on a silicon dioxide substrate. Particles are trapped by local maxima of evanescent waves near the waveguide surface and move in the direction of exciting beam propagation [217]. (b) Formation of a 'photonic nanojet' on the shadow side of a microsphere 3 μm in diameter fixed at the end of an optical fiber [159]. (c) Plasmon optical trap formed by a gap between two apertures in a gold film 50 nm thick at the end of a waveguide [224]. Typical dimensions of the trapped particles are indicated in the figure; λ is the radiation wavelength.

object. As a result, traps based on beams formed by microscope objectives with a high numerical aperture, whose scattering spot diameter is diffraction-limited, become inefficient, and increasing the radiation power can cause thermal destruction of the trapped particle [210, 211]. In turn, reducing the environment viscous friction negatively affects the stability of trapping nanometer particles, because their Brownian motion is considerably enhanced, also reducing the optical trap efficiency.

To solve this problem, attempts were made to increase the localization of the electric field energy in the region to scales much smaller than the diffraction limit at the wavelength of the exciting beam. The principle of reducing the focal spot size in an optical trap below the diffraction limit was first demonstrated in 1996 by the example of evanescent waves [212, 213] near the surface of a circular dielectric waveguide [214]. Surface waves give rise to a gradient force that attracts a particle to the waveguide surface, whereas the scattering force pushes it along the direction of light propagation.

Later on, this approach was used to calculate the operation of an optical trap formed by the overlap of evanescent waves of two parallel silicon waveguides with a rectangular cross section on a substrate [215, 216] for transparent and absorbing particles with a size of 10–65 nm (Fig. 7a). A centuple rigidity increase in such a trap compared to standard trapping schemes was noted for particles of similar sizes and shapes at a beam power of the order of 250 mW. The application of this solution in a lab-on-a-chip system [217] allowed trapping 75-nanometer dielectric particles and SNA molecules in a 100-nm-wide slot between two waveguides. As a result, this scheme was called the 'slot waveguide.' Later, a microring resonator based on a planar waveguide was used to rotate a submicron particle [218, 219].

Dielectric microparticles are also used for subwavelength light focusing [220] with the formation of a photonic nanojet, arising on the shadow side of spheres or cylinders 1–6 μm in diameter made of dielectric materials, such as glass and plastic [157, 158] with a refractive index of < 2. Physically, a photonic jet is formed by a caustic — the envelope of rays refracted and re-reflected in the optically denser medium. The minimum beam width of the created nanojet (Fig. 7b) is about $\lambda/3$ [159], but can be substantially reduced by structuring the microspheres, e.g., making concentric rings on the surface [221] or nanoholes on the shadow surface of a microsphere or cuboid [222, 223].

Reference [158] demonstrated a method for creating a photonic nanojet by a cylinder 6 μm in diameter placed in front of a reflecting surface irradiated by a beam. Multiple refractions and reflections from the surfaces create a characteristic region of standing waves with minima and maxima alternating with a period of $\lambda/2n$, where n is the relative refractive index. Optical tweezers based on this scheme can be used to trap particles with both high and low contrast of the refractive index, providing a wide operating zone for optical trapping. Due to the relative simplicity of technical implementation, optical tweezers based on a photonic nanojet can find practical application in lab-on-a-chip systems for optical sorting and alignment of atoms or nanoparticles.

Along with microspheres, dielectric photonic crystals [225], whose periodic structure transmits radiation at certain frequencies in certain directions or, conversely, suppresses its propagation [226], are more and more widely used to create strong near-surface field gradients. Resonators and waveguides based on photonic crystals open new ways of modulating light fields for trapping a wide range of cell structures and individual molecules of micron and submicron sizes [227].

3.5 Plasmonic optical traps

Interest in studying near-field effects in a near-surface layer of metalls is related to numerous applied problems [228]. In this case, particular attention is devoted to creating conditions for local transformation of the light field and its enhancement in a restricted region due to the energy of plasmons. The main subject of plasmonics is surface plasmons — coupled oscillations of the gas of near-surface electrons and electromagnetic waves.

Surface plasmons, near-field modes localized on the surface of metallic nanostructures, have a sharp intensity gradient in one of several directions and are commonly divided into two categories: surface plasmon polaritons (SPPs) and localized surface plasmons (LSPs). SPPs are surface electromagnetic waves arising at the metal-dielectric interface due to the motion of free metal electrons under the action of an incident field and propagating along the electromagnetic field interface. Exponentially decaying with distance, SSPs create high-intensity localized fields and can concentrate light at scales well below the diffraction limit, which opens new possibilities for trapping nanoparticles. The second type of plasmons, local surface plasmons, are formed due to a resonance near subwavelength metallic structures (antennas or holes of various shapes) as a result of which the optical field is 'restrained' in a region with dimensions much smaller than the wavelength.

The unique properties of surface plasmons offer a base for optical traps that allow superhigh-precision positioning of individual nanoobjects, thus opening unprecedented possibilities in many fields of research [229].

3.6 Traps based on surface plasmon polaritons

The most important advantage of optical trapping using surface plasmon polaritons is the formation of a sharp optical field gradient, even in the case of low power of laser radiation, exciting evanescent waves. Due to this fact, forces

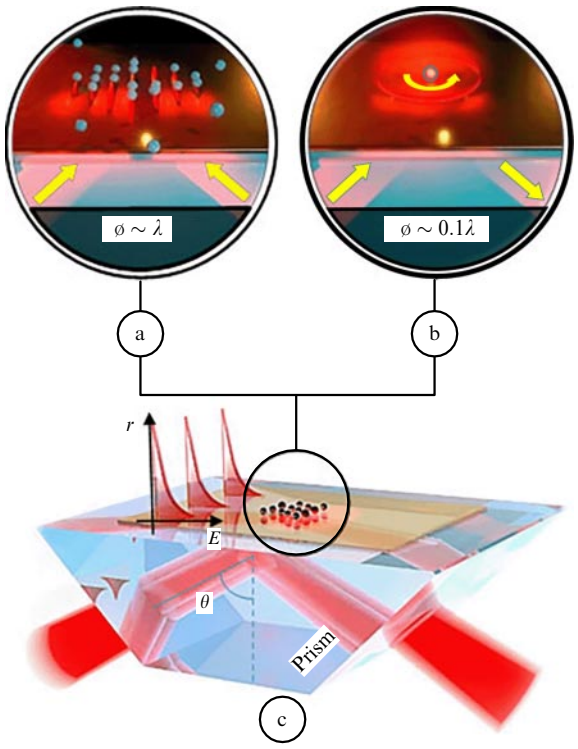

Figure 8. Optical trap formed by surface plasmon polaritons based on the Kretschmann configuration. (a) Counterpropagating laser beams exciting surface waves form a plasmon interference pattern in the form of fringes on the surface of a golden film 50–100 nm thick. Trapping of particles with positive polarizability occurs in the region of plasmon wave maxima [196]. (b) Spiral structure on the surface of the golden film induces 'screwed beams' carrying orbital angular momentum, which imparts rotation to the trapped nanoparticle [234, 235]. (c) Total internal reflection prism with a metallic plate implementing the Kretschmann geometry [231] for exciting surface waves. Typical dimensions of trapped particles are indicated in the figure; λ is the wavelength of the exciting radiation.

of sufficiently high magnitude arise, which are necessary for two-dimensional stable trapping of nanoparticles, at the same time reducing the risk of their optical damage by thermal action as compared to usual optical tweezers [230].

To maintain surface plasmon polaritons, it is necessary to have an electron plasma near the metal surface, as well as a dielectric that ensures the coupling of the plasma with the light wave electromagnetic field. The most used method for exciting surface plasmon polaritons exploits the Kretschmann configuration [231], the main element of which is a glass prism with a thin metallic (mainly gold) film coating on one of the faces involved in the total internal reflection (Fig. 8). The angle θ of the exciting wave incidence determines the condition for the space plasmon resonance, and a small deviation from the resonance angle allows controlling the balance between the scattering force, whose magnitude grows when the angle decreases, and the gradient force (Fig. 8a). As a result, changing the incidence angle ensures fine tuning of the resulting force acting on the trapped nanoparticle [232], which is important, for example, for selective trapping of particles of a given size [233].

Controlling the phase peculiarities and polarization of surface plasmon polaritons attracts particular interest: a number of papers [88, 236] demonstrate the formation of surface plasmon polaritons carrying an orbital angular momentum (Fig. 8b) and possessing a vector field structure. Through gold film ion etching, a spiral structure was formed on its surface, the exposure of which to a circularly polarized beam allowed generating evanescent waves with the orbital angular momentum, trapping by which imparts a rotational motion to a nanoparticle.

Worth noting are also thermal effects caused by the electromagnetic wave absorption because of ohmic losses in the metal, which is an inalienable property of plasmonic devices [219]. Generally, such a phenomenon is harmful to the stable trapping process due to the appearance of thermophoresis [237] and convection [238]. Nevertheless, in some cases, the effect has been used directly to trap colloidal particles [239] and molecules [240, 241]. For detailed information on thermal effects in plasmonic systems and their application to optical trapping and molecular structuring, the reader is directed to recent reviews [242, 243].

3.7 Traps based on localized surface plasmons

When an exciting beam irradiates nanoscale metallic structures whose size is comparable to or less than the wavelength of the incident radiation, a conversion of collective electron oscillations of localized surface plasmons occurs. As a result, a resonance can arise leading to the enhancement of the field at the nanostructure surface. In contrast to surface plasmon polaritons, excited in a wide frequency range, the generation of localized surface plasmons is associated with the frequency of the inducing radiation, which leads to light absorption at the corresponding wavelength. In turn, the resonance frequency is determined by the nanostructure shape and size [224], which allows tuning its characteristics and the efficiency of plasmon generation. To date, the formation of localized surface plasmons for the purpose of optical trapping of nanoparticles is implemented using nanodots [245], nanoantennas [246, 247], nanoresonators [248, 249], and nanoapertures [250, 251] with various shapes and sizes of holes [224]. To prepare such nanostructures, the methods of electron beam and colloidal lithography [252, 253], as well as ion beam etching [254, 255], are most widely used. A separate review devoted to this technology and its capabilities in the creation of plasmonic nanostructures and photonic crystals can be found in Ref. [256].

A characteristic advantage of generating localized surface plasmons is the direct excitation by a focused beam, the power of which can be limited to a few milliwatts. Nevertheless, the dynamics of nanoparticles behavior in such a trap [228] can be determined by the combined action of photophoretic forces and thermal effects [257] due to the absorption of the light energy in the metal [238, 258]. Reference [259] proposes a method of suppressing the thermal effect on trapping particles less than 100 nm in diameter at the expense of the shape of the nanostructures. Reference [260] considers the application of additional substrate layers for the efficient redistribution of heat and increasing the trap efficiency by 30%.

A number of studies in the field of plasmonics led to the understanding of the fact that the resonance frequency of the excited plasmon field is very sensitive to changes in the local refractive index [228]. Therefore, in designing a plasmonic structure, for example, in the form of nanoapertures [261, 262], it is taken into account that the trapped particle itself can dynamically affect the trapping process [263]. When a particle whose refractive index is greater than that of the environment finds itself in the aperture region (Fig. 8c), it changes the resonance characteristics of the aperture [120], thus considerably enhancing light transmission. The resulting change in the momentum of photons creates a burst of

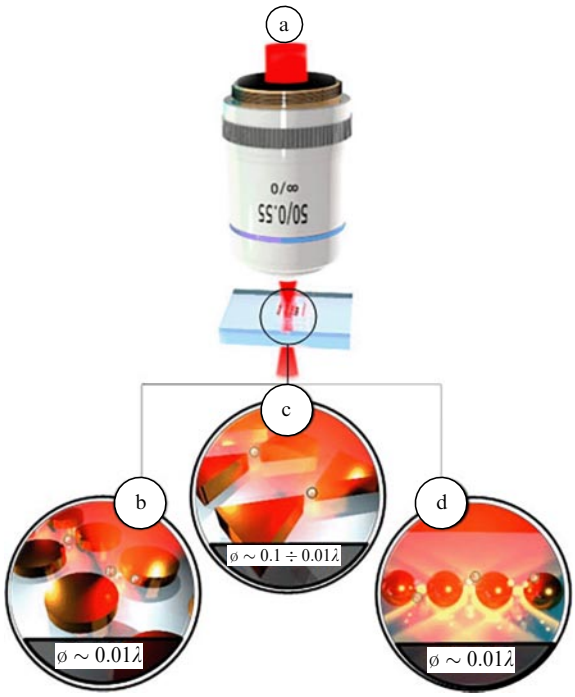

Figure 9. (a) Optical scheme for generating localized surface plasmons for optical trapping of nanoparticles. (b) Plasmonic traps formed near the surface of golden nanodiscs 75 nm in diameter [235]. (c) Nanoantennas with a triangular geometry make it possible to obtain a minimum trapping region at the edges [270–272]. (d) Nanosphere 25 nm in diameter installed on a dielectric substrate with a spacing of 10 nm. Scheme allows stable trapping of dielectric 5-nanometer particles [273]. Typical dimensions of the trapped particles are indicated in the figure. λ is the exciting radiation wavelength.

the gradient force acting on the particle and attracting it to the aperture center. This effect is called self-induced back-action (SIBA) [263]; it allows increasing the nanoparticle trapping efficiency by an order of magnitude [248, 264]. For example, the SIBA effect allowed the stable trapping of a nanoparticle less than 5 nm in diameter by a plasmon nanoantenna placed on a silicon oxide substrate [247], as well as on a waveguide end face [250].

Considering all the advantages of plasmonic optical traps, it is worth noting a number of limitations, too, associated with trapping nanoparticles in a two-dimensional space and with difficulties in controlling their spatial position, which require new approaches to metasurface engineering (Fig. 9) [265–268]. Reviews of modern achievements in this field can be found in Refs [243, 249, 269].

For convenience, Table 2 presents the basic characteristics of optical traps with various configurations.

3.8 Integration of optical trapping with monitoring and optical measurement systems

Applications of optical manipulation systems practically always require monitoring the trapping dynamics and recording the position of the object and the forces acting on it [287]. Along with classical wide-field optical microscopy, depending on the character of the trapped objects and the objectives of the experiment, technologies of three-dimensional imaging are used in combination with optical traps, e.g., confocal [295] and two-photon microscopy [296], digital holography [24, 297–299], Raman microspectroscopy [120, 170, 300], and fluorescence light sheet microscopy [301, 302].

Currently, trapped microparticles a few micrometers or larger in size are observed by means of video registration methods using commercially available digital cameras [303] with a wide range of resolutions and frame rates from 25 Hz or more. The combination of video recording and wide-field microscopy using high-aperture optics is characteristic. Technically, the application of high-speed cameras facilitates the improvement in temporal resolution [304], moreover, the

Table 2. Basic approaches to the formation of optical traps.

Trapped object	Size	Forces	Environment	Beam type	Laser type	Power	Focusing conditions	Reference
Single-beam optical traps								
Absorbing particles (Al_2O_3)	0.5–1.5 μm	Photophoretic forces	Air	Hollow beam	Diode laser, 532 nm	10 mW per trap	100 × objective	[274]
Microspheres of silicon and polystyrene	0.55–3.8 μm	Gradient forces, 9.2 μN at trap power of 100 mW	Water	Gaussian beam	Ti:sapphire laser, 780 nm, pulsed mode (80 MHz)	300 mW (laser); 40–22 mW per trap	60× (NA 0.7) objective	[275]
Polystyrene spheres	0.5–2.1 μm	Gradient forces	Water	Vector beams with radial and azimuthal polarization	Nd:YAG, 1064 nm	—	100× (NA 1.3), 63× (NA 0.7–1.4) objective	[276]
SiO_2 microspheres	1.15 and 2.25 μm	Gradient forces, 15–140 nN	Water	Gaussian beam	Diode laser, 827 nm	—	—	[277]
Cloud of atoms	Trap width 2.5 μm	Light pressure forces	Air	Hollow beam generated by SLM	850 nm	20 mW	Aspherical lens (NA 0.50)	[141]
Gold nanoparticles	1–3 μm × 40 nm	Gradient forces, 4 pN (at 25 mW)	Water	Single-beam trap with strong focusing	Ti:sapphire laser, 800 nm	25–100 mW	60× (NA 1.2)	[278]
Microspheres (latex)	1.2 and 3.2 μm	Gradient forces	Water	Gaussian beam with liquid-crystal modulator	Diode laser, 532 nm	500 mW (laser), 10 mW per trap	100 × objective	[125]

Table 2. (continuation)

Trapped object	Size	Forces	Environment	Beam type	Laser type	Power	Focusing conditions	Reference
Yeast cells	1.75–5 μm	Gradient forces, 1–4.6 pN	Water	Gaussian beam	980 nm	300 mW, 20–50 mW per trap	Focusing by needle-like end of optical fiber	[148]
Microspheres of polystyrene and silicon	4–5 μm	Gradient forces	Water	Gaussian beam	1064 nm	2 W	40× (NA 0.95)	[131]
Red blood cells of a rat	5–6 μm	Gradient forces, 0.5 pN	Blood plasma	Gaussian beam	Nd:YAG laser 1064 nm	20 mW per trap	100× (NA 1.0) objective	[182]
Carbon particles	7–9 μm	Photophoretic forces, 7×10^{-12} N	Air	Airy beams, generated at SLM	Diode laser 532 nm	120 mW (laser), 2–2.5 mW per particle	8× (NA 0.2) objective	[135]
Carbon particles	10 μm	Photophoretic forces	Air	Hollow beam, generated by SLM	Diode laser, 532 nm	500 mW	20× (NA 0.4) objective	[136, 140]
K562 cells	10–15 μm	Gradient forces, 20 pN	Nutrition solution	Hollow beam generated by SLM	Diode laser, 532 nm	200–2000 mW	10× objective	[279]
Microdroplets of glycerol solution in water, 10:90	19.5–24.2 μm	Photophoretic forces	Air	Laguerre–Gaussian beam	Diode laser, 532 nm	1 W, 98–230 mW per trap	Short-focus lenses, $f = 2-8$ mm	[78]
Conglomerate of carbon particles	20–30 μm	Photophoretic forces	Air	Hermite beams and hollow beams	Diode laser, 457 nm and 532 nm	2 W (laser 457 nm) 500 mW (laser 532 nm), 16 mW per trap	3.7× (NA 0.1) objective	[280]
Hollow microspheres with gold coating	25–35 μm	Photophoretic forces: pushing force, 6.7 nN, pulling force, 3.4 nN	Air	Hollow beam with radial and azimuthal polarization	Diode laser, 532 nm	200 mW	Beam diameter in the focal region of 35 μm	[115]
Potorous tridactylus cells (PTK2)	—	Gradient forces, 67–1330 nN	Water	Gaussian beam	Nd:YAG laser, 1064 nm	10–100 mW	—	[281]
Double-beam optical traps								
NaYF4:Er/Yb nanorods	0.14 × 1.47 μm	Gradient forces, 0.122 nN/μm and 0.003 nN/μm	Water	Counterpropagating Bessel beams	Diode laser, 808 nm	26.5–41.5 mW	Beam diameter of 1.64 μm	[147]
Silicon spheres	0.2 μm	Gradient forces, 1 pN	—	Standing waves formed in counterpropagating beams, emitted by waveguides	1550 nm	50 mW	Waveguide width of 3.5 μm	[282]
Bacillus subtilis cells	0.5 μm	Gradient forces, 0.09–0.25 nN	Solution of NaCl	Dynamically controlled beams formed by SLM	Ti:sapphire laser, 790–850 nm	1.5 W (laser) 3–5 mW per trap	100× (NA 1.3) objective	[283]
Glass and silicon microspheres, volcanic ash, sucrose	1–30 μm	Photophoretic forces	Air	Counterpropagating and hollow beams formed by axicons	Diode laser, 488 nm and 532 nm	1 W	Parabolic mirror with $f_1 = 2$ mm (NA 0.92), $f_2 = 19$ mm (NA 0.60)	[119]
Carbon nanotubes	10.51–20.14 μm	Photophoretic forces, 3.30×10^{-10} N	Air	Counterpropagating Gaussian and hollow beams	Diode laser, 405 and 445 nm	3–500 mW per trap	50× (NA 0.55) objective and concave mirror with $f = 10$ mm	[284]
Bermuda smut spores	17.11 μm							
English oak pollen	33.78 μm							

Table 2. (continuation)

Trapped object	Size	Forces	Environment	Beam type	Laser type	Power	Focusing conditions	Reference
Carbon nanotubes and absorbing particles	10–50 μm	Photophoretic forces	Air	Counterpropagating Gaussian beams	445 nm	500–1000 mW (laser), 200 mW per trap	Lens with $f = 25.4$ mm	[164]
Cylindrically shaped micro-instrument	2.5–6 μm	Gradient forces, 2.5–6 nN	Water	SLM-shaped beams	—	—	—	[285]
Diethyl phthalate microdroplets	20–25 μm	Scattering forces	Air	Counterpropagating Gaussian beams	Arion laser, 488 nm	750 mW	Aspherical lens (NA 0.55)	[170, 171]
Hollow glass microspheres	2–4 μm	Gradient forces	Water	Collinear Gaussian beams	Nd:YAG laser, 1064 nm	500 mW (laser), 30–120 mW per trap	20× objective	[286]
Glass rods	1.5–30 μm							
Microdroplets of glycerol aqueous 10:90 solution	29.9–40 μm	Light pressure forces	Air	Counterpropagating Gaussian beams	Diode laser, 532 nm	2 W (laser), 350 mW per trap	$f = 5$ mm objective	[168]
Microrotor (impeller)	3 μm	Gradient forces, 1 pN, torque, 10 nN μm	Water	Gaussian beams formed by SLM	Fiber laser CW Yb, 1070 nm / Ti:sapphire laser, 780 nm	40 mW	100× (NA 1.3)	[192]
Multi-beam optical traps								
Silicon spheres	1–10 μm	Gradient forces, 5–15 nN	Water	Holographic trap	Fiber laser, 104 nm	10 W	60× (NA 1.2)	[287]
Silicon spheres	1.5 μm	Gradient forces	Water	Holographic trap	Solid-state laser, 532 nm	5 W (laser), 3 mW per trap	100× (NA 1.4)	[288]
Microrotors	2–5 μm	Gradient forces	Water	Holographic trap	Solid-state laser, 1064 nm	3 W	100× (NA 1.3)	[289]
Silicon spheres								
Yeast cells								
Silicon spheres	2–5 μm	Gradient forces, 100 nN	Water	Holographic trap	Solid-state laser, 515 nm	3 W (laser), 100 mW per trap	100× (NA 1.3)	[290]
Polystyrene spheres	3–5 μm	Gradient forces	Water	Holographic trap	Ti:sapphire laser, 785 nm	0–800 mW (laser), 3–50 mW per trap	60× (NA 1.2)	[291]
Pseudomonas Aeruginosa bacteria								
Saccharomyces Cerevisiae yeast cells								
Red blood cells								
E-lymphocytes								
Dielectric particles	3 μm	Gradient forces	Water	Holographic trap	Fiber laser, 1064 nm	40–60 mW per trap	100× (NA 1.40)	[292]
Yeast cells	10–12 μm	Gradient forces	Buffer solution	Gaussian beams formed by SLM	Diode laser, 532 nm	800 mW	100× (NA 1.4) objective	[56]
Murine embryonal stem cells	8–12 μm	Gradient forces	Nutrition solutions	Holographic trap	1064 nm	30 mW per trap	40× (NA 1.3), 100× (NA 1.3)	[202]
Optical traps based on evanescent waves								
Spheres (Au)	20–50 nm	Gradient forces, 28 fN	Water	'Photonic jet' interference of beams	1550 nm	1 mW per trap	In the focus of a cylinder 6 μm in diameter with $n = 1.45$	[158]

Table 2. (continuation)

Trapped object	Size	Forces	Environment	Beam type	Laser type	Power	Focusing conditions	Reference
Nanoparticles (Au)	5–15 nm	Gradient forces, $10^{-15}-10^{-27}$ N	—	Surface waves near an aperture	600 nm	10 W	Cuboid with 20-nm hole	[223]
Nanoparticles (Au)	100–150 nm	Gradient forces, 150–200 fN	Water	Surface plasmons formed at two wavelengths	Diode-pumped solid-state laser, 532 nm and 671 nm	0.15–0.2 mW μm^{-2}	100× (NA 1.49) objective	[293]
Polystyrene spheres	1.5 μm	Gradient forces, 7–12 nN μm^{-1} mW^{-1}	Solutions with various pH	Localized plasmons formed by an array of nanoantennas (Au) 425 nm in size with 20 nm spacing	Diode laser, 685 nm	1.0 mW μm^{-2}	40× (NA 0.6)	[272]
Nanoparticles (Au)	10–20 nm	Gradient forces	Water	Localized plasmons formed by nanoantennas 90 nm long with 5–30-nm spacing	808 nm	0.8 W	60× (NA 1.45)	[270]
Dielectric particles	5 nm	Gradient forces, 1–7 nN	Water	Localized plasmons formed by nanospheres (Au), radius of 5 nm	800 nm	—	(NA 1.2)	[294]
λ-DNA	75 nm	Gradient forces, 10–25 nN (normalized to 1 W of radiation power)	Buffer solution	Evanescent waves formed by waveguides with 450 nm cross section and spacing of 60, 100, and 120 nm	1550 nm	250–300 mW	—	[217]
Polystyrene nanoparticles	100 nm							
Polystyrene nanoparticles	20–40 nm	Gradient forces, 2.5 nN μm^{-1} × 100 mW^{-1}	Water	Localized plasmons formed by nanoholes in a film (Au) 277.4 nm in diameter spaced by 44.4 nm	940–980 nm	0.57 mW μm^{-2}	100× (NA 1.33)	[224]
Polystyrene nanoparticles	1.2 μm and 300 nm	Gradient forces, 14 nN μm^{-1} mW^{-1}	—	Localized plasmons formed by triangle-shaped nanoantennas (Au) 50 nm thick, dimensions of 260 × 80 nm	Ti:sapphire laser (pulsed), 100 fs, 80 MHz, 800 nm	65–70 mW (20 mW μm^{-2})	40× (NA 0.6)	[246, 271]
Nanoparticles (Au)	80 nm							
Polystyrene nanoparticles	20 and 30 nm	Gradient forces	Water	Localized plasmons formed by nanoapertures (Au) with 225×175 nm, in size, 100 nm thick, spaced by 70 nm	980 nm	50 mW (0.5 mW μm^{-2})	—	[250]
CdSe/ZnS particles	4.0 nm	Gradient forces, 11.2 nN	Water	Localized plasmons formed by nanoapertures (Au), 200×160 nm in size, 100 nm thick, spaced by 5, 8, and 10 nm	1560 nm	40 mW (1.27 mW μm^{-2})	60× (NA 0.65)	[247]
Dielectric microparticles	1 μm	Gradient forces, 0.6–3 nN	Water	Surface plasmons formed by Archimedean spiral on a nanolayer of Au 250 nm thick. Spiral thickness of 300 nm, diameter of 2.5 μm	1545 nm	40–80 mW	Aspherical double-convex lens, $f = 5$ cm	[88]

spatial resolution often lowers with an increase in the frame rate [305]. The use of special algorithms of image processing [306], in turn, allows subpixel accuracy in positioning the trapped particle to units of nanometers [229].

Recent advances in the field of visualization and optical beam spatial modulation technology allow microparticle observation and manipulation even in strongly scatterad media and at a substantial depth [307, 308], which makes the camera-recording method the most requested in tasks of optical manipulation with an ensemble of particles. In the case of trapping single particles, the method that is easiest to work with is detecting the particle position in a trap using quadrant photodetectors (QPDs) — semiconductor four-sector photodiodes operating at frequencies up to a few kilohertz [309, 310].

The use of wide-field microscopy *in vivo* can lead to certain difficulties due to the large physical dimensions and the limited degrees of freedom of optical elements. The endoscopic approach based on using optical fibers, for instance, fiber fluorescence microscopy, allows substantial simplification of the trapped particle tracing procedure [311]. At the same time, label-free fluorescence microscopy, for example, Raman spectroscopy [300], is becoming the most requested solution for the noninvasive monitoring of living objects.

Combining optical tweezers with fluorescence analysis significantly increases the optical trapping efficiency in a large number of applied studies. In particular, in the tasks of analyzing physical and chemical properties and the evolution of individual cells, Raman tweezers — a combination of Raman spectroscopy as a diagnostic tool at the molecular level and optical tweezers — became a widespread solution in medical and biological research [312, 313]. An advantage of this symbiosis consists in the specific fluorescence quenching in an optically trapped particle as compared to the case as if it was located on a substrate. This principle was successfully exploited in studies of fast chemical processes in atmospheric aerosols [170, 171, 300]. In Ref. [314], the possibility of forming a $6 \times 6 \times 4$-μm spatial structure of particles of different natures, including *E. coli* bacteria, was demonstrated in a gelatin matrix by means of a holographic optical manipulator. Raman spectroscopy of the obtained structure provided information on the vitality of a colony of bacteria over a long period of time.

As a separate example of fluorescence microscopy using optical traps, let us consider so-called 'light sheet fluorescence microscopy' [302, 315]. The advantage of this method is the minimum optical damage to the object under study because of the reduced area of fluorescence-inducing field action. The detection of the fluorescence signal in this case occurs in the direction orthogonal to that of the exciting and trapping beams, which allows using the latter as the fluorescence beam.

The phenomenon of Föster resonance energy transfer (FRET) in combination with optical trapping was studied in Ref. [316]. Such an approach allowed investigating the peculiarities of the mechanical action of the environment on cell populations and the process of external excitation conversion into biochemical signals [229].

As a separate issue, the rapidly developing methods of three-dimensional microscopy of optically trapped microparticles can be distinguished. The authors of Ref. [317] demonstrated a combination of holographic optical tweezers with the possibility of remote axial scanning of the trapping region up to 66 μm long by an aberration-suppressed system of microscope objectives [318].

Using interference methods in combination with the principles of digital processing of phase portraits and holograms opens new possibilities in interferometry and three-dimensional reconstruction of the surface geometry of optically trapped samples and its morphological peculiarities at the micro- and nanoscopic levels. The value of digital holographic microscopy as a powerful tool for tracking the spatial position of particles consists in the ability to monitor a sufficiently large volume of the preparation, from tens of micrometers to a few millimeters, in combination with high axial resolution, to tens of nanometers [319, 320].

Decades of rapid development of digital holography as an applied method in microscopy made it possible to use numerous algorithms of image computer processing, including neuron networks [321, 322]. The most in demand is the approach of numerical focusing instead of mechanical, for which one hologram is sufficient [323, 324]. Holographic microscopy became widely used in studies of aerosol particles and their interaction in optical traps [325, 326]. In this case, the main difficulty that restricts the application of digital holographic microscopy arises when working with turbid media or at high particle concentrations.

The application of digital holographic microscopy principles to probing a trapped particle with a beam directed at various angles [327] makes it possible to obtain a set of optical path length values and to reconstruct the refractive index spatial distribution. This allows calculating various derivative characteristics, such as density, concentration, and morphometric indicators (for biological samples). For this purpose, local tomographic phase microscopy (TGM) has been intensely used over the last decade [328, 329].

Currently, the THM method is becoming widely used as microscopy free of auxiliary labels and contrast agents for measuring the three-dimensional refractive index, which opens up new opportunities for studying intracellular dynamics and biochemical analysis [330]. There are two approaches to the formation of a phase distribution aimed at restoring information about the local distribution of the refractive index: scanning with a laser beam [331] and rotating the sample itself [327].

A combination of optical trapping and TGM offers new possibilities for noncontact interaction with objects studied *in vivo*. For example, optical rotating traps based on fiber optics [63], astigmatic beams [54], and micromachines [56] can ensure angular orientation of the samples under study in an aqueous solution for TGM needs [58, 332].

4. Application of optical traps in medicine and biology

The widespread use of optical trapping in biological research, in particular, for positioning, modifying, and sorting various biological objects, gave impetus to the development of trapping-based optical measurements. It is known that, when being optically trapped, an object contributes to the intensity of the light beam and the direction of its scattering or refraction. This principle grounds the traps with feedback. Using these features, one can analyze the quantitative characteristics of the biological sample structure, as well as sort them depending on the morphological properties. For example, Ref. [333] demonstrated an approach to analyzing the mechanical properties of DNA molecules: one end of a DNA molecule was attached to a glass surface by means of an RNA polymerase complex and the other end was connected

to a microscopic ball captured in an optical trap. Then, the DNA molecule was stretched by moving the glass with respect to the trap using a piezo-controlled translator, while the position of the ball remained fixed.

Reference [334] describes a method of direct measurement of volume variation in an isolated kidney cell under an ascending (osmotic) shock and a phenomenological analysis of water transfer with the osmoregulation taken into account. In the course of the experiment, a cell of the kidney tissue was captured in an optical trap and kept in a suspended condition without contact with the glass substrate on which the sample was placed. This approach allowed measuring the cell volume by leveling the influence of intercellular interaction and environment.

Spectrometry is one of the methods to get information about the condition of a cell captured in an optical trap. In Ref. [335], optical tweezers were used in real-time mode in combination with the measurement of spectral characteristics, which allowed determining quantitative indexes of enzymatic processes inside a yeast cell. In Ref. [336], this technique was applied to identify six kinds of bacteria in various environments. Moreover, this method allows distinguishing cancer and healthy cells [337], as well as typical and modified lymphocytes [338]. In Ref. [339], optical tweezers and a Raman fluorescence microscope were used to explore the effect of curvature gradients caused by optical stretching of single-layer vesicles.

Optical tweezers allow noninvasive transportation of living organism cells in various media. For example, in Ref. [340] optical tweezers were used to form a group of neurons. The flask for cultivating the cells was divided into two halves. The first half was coated with a glue layer, and the second one was made less adhesive by applying a thin elastomer layer. The neuron cells not attached to the flask surface were captured in an optical trap and carried to attached cells on the adhesive surface. Optical trapping did not affect the subsequent ability of neurons to attach to the cultivated substrate. Sixty percent of trapped cells survived for two or more days, and their structure was not damaged.

Optical tweezers are also used to determine the properties of bacteria. Reference [340] describes an experiment in which the comparison of genetically similar cells was demonstrated without mixing the media. A narrow channel connected two chambers with each other. In the first chamber, a bacterium divided into two cells. One of the cells was then optically trapped and through the narrow channel was brought to the other chamber, where its further growth and cultivation occurred. The method can be used to assess the influence of the environment itself on various cells. Reference [341] showed that the optimal stability of optical trapping is achieved when the trap length is proportional to the length of the trapped bacterium.

Another area of optical trap application is active and passive cell sorting. Active sorting uses various labels, e.g., fluorescent ones. Passive sorting is based on the morphological properties of cells. As a rule, in experiments, two chambers connected by a channel are used. The cell is analyzed when passing through the channel, after which the cells are sorted using optical traps [342]. However, interest in cell sorting by optical traps remains. For example, in Ref. [343], a Raman-based automatic cell sorting system is reported in which optical tweezers are used to sort individual cells of interest from microbial communities by their Raman spectra. Such sorting of cells and the consequent analysis of their DNA, for example, by metagenomics, known as a single-cell genomics, or cultivation allow establishing a direct relation between the metabolic roles and genomes of microbial cells in complex microbial communities, as well as implementing targeted extraction of new microbes with a certain physiology.

In Ref. [344], cells were sorted by the type of fluorescence emission. Suitable cells were trapped and redirected to the appropriate channel. The rest of the cells continued the initial motion in the flow. In Ref. [345], the separation of red blood cells and lymphocytes based on their morphological features was demonstrated. Using optical multibeam traps, one can sort a few cells simultaneously and form complex structures from a group [346]. A promising line of research is the parallel trapping of groups of cells. Cells and other biological objects (e.g., vesicles, liposomes) [347, 348] can merge in a single structure upon very close contact followed by a rapid change in temperature. Single-beam or double-beam optical traps allow keeping cells in precisely specified spatial positions, then the cells are subjected to a fast photothermal pulse, as a result of which the biological objects merge into a single structure.

4.1 Application of optical traps in biology and medicine: problems and prospects

When using optical traps to capture and study living objects, a number of different parameters are to be taken into account, and when interpreting the experimental results, one should not rule out the ability of the optical trap to change the trapped object's structure or biochemistry. Therefore, when carrying out studies on optical trapping of living objects (cells or bacteria), it is also necessary to investigate the process of heating of these objects during the time they spend in the optical trap (Fig. 10). In a paper on studying the mechanical properties of the DNA molecule [333], it was shown that a living sample in an infrared optical trap is heated insignificantly. Therefore, the samples can be damaged only if kept for a long time in an optical trap with a power from 50 to 100 mW.

In Reference [349], the clonal growth (multiplication of single cells) of Chinese hamster ovary cells using an Nd:YAG and tunable Ti:sapphire laser optical traps was studied. The optical trapping forces affected the cell nuclei at different wavelengths, density, power, and duration of exposure. The clonal growth usually decreased with an increase in the energy density and duration of laser exposure, as a result of which a dependence of the clonal growth rate on the wavelength was observed. In Ref. [350], *Escherichia coli* bacteria were attached to glass with flagella. In the wavelength range from 830 to 870 nm and from 930 to 970 nm, critical photoinduced cell damage was revealed, which could be reduced to the background level under anaerobic conditions. The photoinduced damage intensity dependence was linear, which indicates a single-photon process.

To avoid photoinduced damage to biological samples, the method of indirect trapping is used [351]. A silicon ball is attached to a cuvette wall, the cell is captured together with the ball, and the radiation acts on the ball, while the cell remains almost unaffected by the radiation. One more method to minimize the harmful effect of optical radiation on living cells entails using optical micromachines to reduce direct action on the object of study [29].

Damage to living samples was also observed when using optical traps at wavelengths of 800 nm or shorter, for instance, in studies of human spermatozoid cells [352].

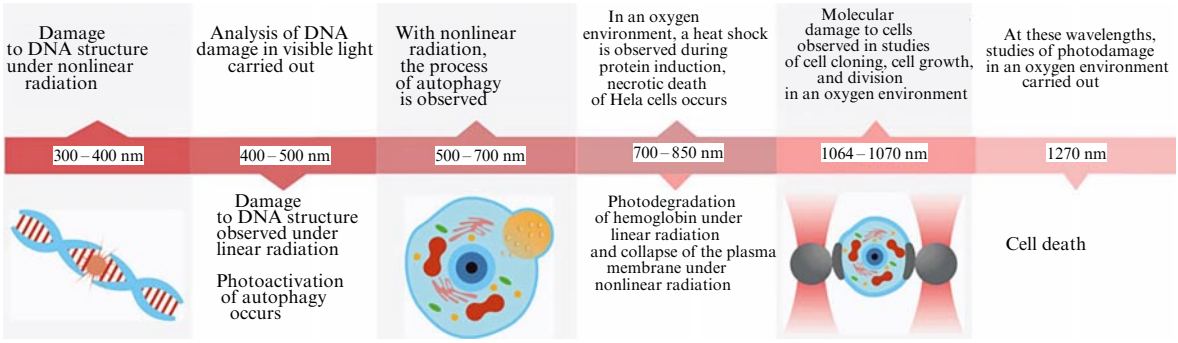

Figure 10. Damage to biological samples in optical traps depending on the wavelength [349, 353, 356–372].

Reference [353] describes side effects of optical traps acting of living *Caenorhabditis elegans* cells under various conditions. It was found that the expression of genes was most often caused by a wavelength of 760 nm, more rarely by 810 nm. The stress reaction increased with the growth of the laser power and duration of exposure. In a wavelength range of 700–760 nm, the stress reaction is due to photochemical processes, whereas, at the wavelength of 810 nm, it is mainly of photothermal origin.

In addition to photothermal and photochemical processes, an oxygen environment can affect an optically trapped cell. For example, in Ref. [354], optical traps were used to characterize the oxygenation response to an external mechanical force of individual healthy and sickle-shaped cells, as well as red blood cells of umbilical cord blood. For all three types of cells, an increase in the laser power (or mechanical force) caused greater cell deoxygenation. However, sickle-shaped erythrocytes deoxygenized faster than normal erythrocytes under the action of similar optical forces. On the contrary, the umbilical cord blood erythrocytes were able to support oxygenation better than normal erythrocytes. These results imply that the difference in chemical or mechanical properties between fetal, normal, and sickle-shaped cells affect the degree to which the applied mechanical forces can deoxygenate a cell. Populations of normal, sickle-shaped, and umbilical erythrocytes were identified and extracted based on this mechanochemical phenomenon.

Damage to biological objects is possible not only under direct action, but also upon sample scanning. For example, in Ref. [355], optical tweezers were used to scan individual cells of chronic myelogenous leucosis in order to determine whether cell death depends of various scanning conditions. The cell mortality was shown to increase sharply at certain frequencies and amplitudes of screening, whereas other frequencies or amplitudes were less harmful.

Although optical traps have some drawbacks when applied to biological samples, the manipulations they make possible are highly sought after in many fields of medicine and biology. By correctly choosing the radiation wavelength and reducing the exposure, one can minimize or completely eliminate their harmful influence on living samples [373, 374].

To finalize, it is worth noting that further improvement in the optical tweezer technique considerably affected the development of practically significant studies in the fields of biology and medicine, e.g., the study of the mechanics of erythrocyte membranes or the interaction of cells and cell components. This greatly facilitated understanding their role in regulating the growth, evolution, and interaction of cells, as well as the effect of various pathological and physiological factors on them [375].

Based on certain advantages and the numerous merits of optical traps in studying the characteristics of various biological objects, it is possible to predict that methods of study based on optical traps will have high potentialities of application in future investigations of the mechanisms and origin of erythropoiesis. Other promising applications of optical traps in erythropoiesis include the development of therapy based on stem cells, the creation of systems of blood cell development *in vitro*, and assistance in the transplantation of exogenous erythrocyte factories into bone marrow to replace damaged endogenous cells for ensuring the supply of erythrocytes. As in the case of any other tool, the optical trap technique in biological studies has its advantages and drawbacks. The wavelength and the trapping force are restricted by potential thermal and nonthermal damage caused by the action of light [376]. The difficulties of using optical traps *in vivo* arise due to the limited penetration depth of laser radiation into biological tissues [17, 377].

Overall, future prospects for developing techniques for studying blood cells based on optical traps can be divided into two branches. On the one hand, there is the realization of new systems presenting a symbiosis of optical tweezers and spectroscopy methods, as well as microscopy techniques or using microfluidic devices in combination with optical traps aimed at increasing the productivity, visualization, and implementation of studies *in vivo*. On the other hand, we have the realization of systemic models of screening and diagnostics of diseases using optical tweezers and manipulators. The simultaneous application of laser knives and optical tweezers allows designing unique noninvasive tools for biology and genetics. For example, in Ref. [378], optical tweezers were used to move chromosome fragments cut out by a laser within a living cell in order to obtain new combinations of them.

It is worth noting that one of the most actively progressing fields of modern research is combining optical and acoustic traps. Optical-acoustic tweezers can produce a force a few orders of magnitude greater than their purely optical counterparts at equivalent power. Reference [379] shows selective manipulation and positioning of single human cells in a standard environment without affecting their viability. In turn, Ref. [380] presents the concept of trapping gas microbubbles with a lipid shell *in vivo*.

5. Conclusion

This review presents only a part of the entire variety of modern optical traps and manipulators that exist and are in use. The up-to-date studies described in the review emphasize the significance of this tool in the development of modern

lines of applied research in biology, medicine, physics, mechanics, robotization, and microscopy.

This study was carried out with financial support from the Russian Foundation for Basic Research within the framework of research project no. 20-12-50301. Section 3.8, "Integration of optical trapping with monitoring and optical measurement systems," was prepared with financial support from the Russian Scientific Foundation within the framework of research project no. 20-72-00065.

References

1. Kepler J *De cometis libelli tres* (Augsburg, Germany: Augustae Vindelicorum, 1619)
2. Lebedew P *Ann. Physik* **311** 433 (1901)
3. Fabrikant V *Usp. Fiz. Nauk* **42** 282 (1950)
4. Kravets T G *Usp. Fiz. Nauk* **46** 306 (1952)
5. Ragulsky V V *Phys. Usp.* **54** 293 (2011); *Usp. Fiz. Nauk* **181** 307 (2011)
6. Nichols E F, Hull G F *Astrophys. J.* **17** 315 (1903)
7. Gaponov A V, Miller M A *Sov. Phys. JETP* **7** 515 (1958); *Zh. Eksp. Teor. Fiz.* **34** 751 (1958)
8. Gaponov A V, Miller M A *Sov. Phys. JETP* **7** 168 (1958); *Zh. Eksp. Teor. Fiz.* **34** 242 (1958)
9. Solunin S A, Solunin A M, Solunin M A *Sov. Phys. Tech. Phys.* **35** 661 (2009); *Pis'ma Zh. Tekh. Fiz.* **35** (14) 48 (2009)
10. Ashkin A *Phys. Rev. Lett.* **24** 156 (1970)
11. Ashkin A et al. *Opt. Lett.* **11** 288 (1986)
12. Zhang H, Liu K-K *J. R. Soc. Interface* **5** 671 (2008)
13. Dai X et al. *Nat. Commun.* **12** 1292 (2021)
14. Swank D M et al. *J. Biol. Chem.* **276** 15117 (2001)
15. Gardini L et al. *Nat. Commun.* **9** 2844 (2018)
16. Ahmadi A, Reihani S N S *Opt. Lett.* **38** 685 (2013)
17. Zhong M-C et al. *Nat. Commun.* **4** 1768 (2013)
18. Lamstein J et al. *Chin. Opt. Lett.* **15** 030010 (2017)
19. Wei H, Amrithanath A K, Krishnaswamy S *IEEE Photon. Technol. Lett.* **31** 599 (2019)
20. Caño-García M et al. *Sci. Rep.* **8** 15804 (2018)
21. Devlin R C et al. *Opt. Express* **25** 377 (2017)
22. Enger J et al. *Lab Chip* **4** 196 (2004)
23. Keloth A et al. *Micromachines* **9** 434 (2018)
24. Miccio L et al. *Opt. Micro-Nanometrology* IV **8430** 84300W (2012)
25. Chen H et al. *Proc. SPIE* **9164** 91641M (2014)
26. Toussaint K C et al. *Opt. Photon. News* **26** 24 (2015)
27. Ghosh S, Ghosh A *Nat. Commun.* **10** 4191 (2019)
28. Soifer V A, Kotlyar V V, Khonina S N *Phys. Part. Nucl.* **35** 733 (2004); *Fiz. Elem. Chast. At. Yad.* **35** 1368 (2004)
29. Andrew P-K, Williams M A K, Avci E *Micromachines* **11** 192 (2020)
30. Kalantarifard F et al. *Nat. Commun.* **10** 2683 (2019)
31. Zemánek P et al. *Adv. Opt. Photonics* **11** 577 (2019)
32. Harada Y, Asakura T *Opt. Commun.* **124** 529 (1996)
33. Chaumet P C, Nieto-Vesperinas M *Opt. Lett.* **25** 1065 (2000)
34. Nieminen T A et al. *Meth. Cell Biol.* **82** 207 (2007)
35. Ashkin A *Biophys. J.* **61** 569 (1992)
36. Zheng H et al. *Phys. Rev. B* **103** 035103 (2021)
37. Gouesbet G, Gréhan G *Generalized Lorenz–Mie Theories* (Berlin: Springer, 2011)
38. Borghese F, Denti P, Saija R *Scattering from Model Nonspherical Particles*: *Theory and Applications to Environmental Physics* (Berlin: Springer, 2007)
39. Pesce G et al. *Eur. Phys. J. Plus.* **135** 949 (2020)
40. Miyata H *Tanpakushitsu Kakusan Koso* **42** 1170 (1997)
41. Volpe G *Contemp. Phys.* **52** 379 (2011)
42. Galajda P, Ormos P *Appl. Phys. Lett.* **78** 249 (2001)
43. Zhang S et al. *Nat. Commun.* **12** 5349 (2021)
44. Bustamante C J et al. *Nat. Rev. Meth. Primers* **1** 25 (2021)
45. Ahn J et al. *Nat. Nanotechnol.* **15** 89 (2020)
46. Manjavacas A, García de Abajo F *J. Phys. Rev. A* **82** 063827 (2010)
47. Zhang Z, Kimkes T E P, Heinemann M *Sci. Rep.* **9** 19086 (2019)
48. Yang D et al. *Opt. Lett.* **43** 4594 (2018)
49. Donato M G et al. *Nano Lett.* **19** 342 (2019)
50. Brzobohatý O et al. *Opt. Express* **23** 7273 (2015)
51. Basudev R et al. *Soft Matter* **12** 5077 (2016)
52. Bezryadina S A et al. *Light Sci. Appl.* **5** e16158 (2016)
53. Lenton I C D et al. *Front. Bioeng. Biotechnol.* **8** 602797 (2020)
54. Mohanty S K, Gupta P K *Methods Cell Biol.* **82** 563 (2007)
55. Villangca M et al. *Light Sci. Appl.* **5** e16148 (2016)
56. Shishkin I et al. *Micromachines* **11** 90 (2020)
57. Gibson G M et al. *Rev. Sci. Instrum.* **83** 113107 (2012)
58. Habaza M et al. *Opt. Lett.* **40** 1881 (2015)
59. Stickler B A et al. *Phys. Rev. A* **94** 033818 (2016)
60. Lin J, Li Y *Appl. Phys. Lett.* **104** 101909 (2014)
61. Bruce G D, Rodríguez-Sevilla P, Dholakia K *Adv. Phys. X* **6** 1838322 (2021)
62. Xiao G et al. *IEEE Photon. J.* **8** 2517131 (2016)
63. Chen X et al. *Opt. Express* **24** 7575 (2016)
64. Nye J F, Berry M V *Proc. R. Soc. Lond. A* **336** 165 (1974)
65. Poynting J H *Proc. R. Soc. Lond. A* **82** 560 (1909)
66. Beth R A *Phys. Rev.* **50** 115 (1936)
67. Ahn J et al. *Phys. Rev. Lett.* **121** 033603 (2018)
68. Kuhn S et al. *Optica* **4** 356 (2017)
69. Hoang T M et al. *Phys. Rev. Lett.* **117** 123604 (2016)
70. Zhong C, Robicheaux F *Phys. Rev. A* **95** 053421 (2017)
71. Rodríguez-Sevilla P et al. *Adv. Biosyst.* **3** 1900082 (2019)
72. Wulff K D, Cole D G, Clark R L *Appl. Opt.* **47** 6428 (2008)
73. Allen L et al. *Phys. Rev. A* **45** 8185 (1992)
74. Courtial J, Padgett M J *Opt. Commun.* **173** 269 (2000)
75. Simpson N B et al. *Opt. Lett.* **22** 52 (1997)
76. O'Neil A T, Padgett M J *Opt. Commun.* **185** 139 (2000)
77. Garcés-Chávez V et al. *Phys. Rev. Lett.* **91** 093602 (2003)
78. Ivanov M, Hanstorp D *Opt. Commun.* **427** 152 (2018)
79. Lamperska W, Masajada J, Drobczyński S *Exp. Fluids* **62** 128 (2021)
80. Xin H et al. *Adv. Mater.* **32** 2001994 (2020)
81. O'Neil A T et al. *Phys. Rev. Lett.* **88** 536011 (2002)
82. Barnett S M N B et al. *J. Opt.* **18** 064004 (2016)
83. Reimann R et al. *Phys. Rev. Lett.* **121** 033602 (2018)
84. Bekshaev A, Vasnetsov M, in *Twisted Photons*: *Applications of Light with Orbital Angular Momentum* (Eds J P Torres, L Torner) (New York: Wiley-VCH Verlag, 2011) Ch. 2, https://doi.org/10.1002/9783527635368.ch2
85. Friese M E J et al. *Phys. Rev. A* **54** 1593 (1996)
86. Angelsky O V et al. *Opt. Express* **20** 3563 (2012)
87. Li M et al. *Phys. Rev. A* **97** 053842 (2018)
88. Tsai W-Y, Huang J-S, Huang C-B *Nano Lett.* **14** 547 (2014)
89. Tkachenko G et al. *Optica* **7** 59 (2020)
90. Zhang Y et al. *Opt. Express* **27** 12414 (2019)
91. Shvedov V G et al. *Opt. InfoBase Conf. Pap.* **19** 273 (2011)
92. Porfirev A P, Shipilov A S *CEUR Workshop Proc.* **1638** 111 (2016)
93. Gong L et al. *Sci. Rep.* **6** 29001 (2016)
94. Suarez R A B et al. *Opt. Lett.* **45** 2514 (2020)
95. Lenton I C D et al. *Opt. Commun.* **459** 124864 (2020)
96. Pan Y -L et al. *Appl. Phys. Lett.* **104** 113507 (2014)
97. Rohatschek H *J. Aerosol Sci.* **16** 29 (1985)
98. Jovanovic O *J. Quant. Spectrosc. Radiat. Transf.* **110** 889 (2009)
99. Zhang Y et al. *Phys. Rev. Lett.* **121** 133901 (2018)
100. Sukhov S, Dogariu A *Phys. Rev. Lett.* **107** 203602 (2011)
101. Ding W et al. *Adv. Photon.* **1** 024001 (2019)
102. Li X et al. *Sci. Adv.* **5** eaau781 (2019)
103. Fernandes D E, Silveirinha M G *Phys. Rev. A* **91** 061801 (2015)
104. Gao D et al. *Laser Photon. Rev.* **9** 75 (2015)
105. Novitsky A, Qiu C-W, Lavrinenko A *Phys. Rev. Lett.* **109** 023902 (2012)
106. Brzobohatý O et al. *Nat. Photon.* **7** 123 (2013)
107. Novitsky A, Qiu C-W, Wang H *Phys. Rev. Lett.* **107** 203601 (2011)
108. Mizrahi A, Fainman Y *Opt. Lett.* **35** 3405 (2010)
109. Alaee R, Christensen J, Kadic M *Phys. Rev. Appl.* **9** 014007 (2018)
110. Kajorndejnukul V et al. *Nat. Photon.* **7** 787 (2013)
111. Lepeshov S, Krasnok A *Optica* **7** 1024 (2020)
112. Li G et al. *Opt. Mater. Express* **6** 388 (2016)
113. Novitsky A et al. *Sci. Rep.* **7** 652 (2017)
114. Lu J et al. *Phys. Rev. Lett.* **118** 043601 (2017)
115. Shvedov V et al. *Nat. Photon.* **8** 846 (2014)
116. Sukhov S, Dogariu A *Rep. Prog. Phys.* **80** 112001 (2017)
117. Li H et al. *Adv. Opt. Photonics* **12** 288 (2020)
118. Zhang X, Yang S, Yuan L *Chin. Opt. Lett.* **17** 090603 (2019)

119. Pan Y-L et al. *Opt. Express* **27** 33061 (2019)
120. Lou Y, Wu D, Pang Y *Adv. Fiber Mater.* **1** 83 (2019)
121. Gong Z et al. *J. Quant. Spectrosc. Radiat. Transf.* **214** 94 (2018)
122. Wu M-Y et al. *Sci. Rep.* **7** 42930 (2017)
123. Stuhrmann B et al. *Rev. Sci. Instrum.* **77** 063116 (2006)
124. Smalley D E et al. *Nature* **553** 486 (2018)
125. Korobtsov A V et al. *J. Opt.* **16** 035704 (2014)
126. Khonina S N et al. *Comput. Opt.* **43** 756 (2019)
127. Pavelyev V et al. *Appl. Opt.* **51** 4215 (2012)
128. Porfirev A P, Skidanov R V *Opt. Trapp. Opt. Micromanipulation XI* **9164** 91643A (2014)
129. Sokolovskii G S et al. *J. Phys. Conf. Ser.* **572** 012039 (2014)
130. Sokolovskii G S et al. *Prog. Quantum Electron.* **38** 157 (2014)
131. Liang Y et al. *Rep. Prog. Phys.* **83** 032401 (2020)
132. Simpson N B et al. *J. Mod. Opt.* **45** 1943 (1998)
133. Mitri G F *J. Opt.* **18** 105402 (2016)
134. Porfirev A P, Skidanov R V *J. Opt. Technol.* **82** 587 (2015)
135. Porfirev A P *Appl. Opt.* **60** 670 (2021)
136. Porfirev A *Opt. Eng.* **59** 055109 (2020)
137. Bo H et al. *Appl. Phys. Express* **11** 052501 (2018)
138. McDougall C et al. *Opt. Trapp. Opt. Micromanipulation IX* **8458** 845824 (2012)
139. Skidanov R V, Porfirev A P, Ganchevskaya S V *Komp'yut. Opt.* **38** 717 (2014)
140. Porfirev A P, Skidanov R V *Opt. Express* **23** 8373 (2015)
141. Barredo D, Lienhard V, Scholl P *Phys. Rev. Lett.* **124** 023201 (2020)
142. Liu Z et al. *Opt. Express* **14** 12510 (2006)
143. Zhao X et al. *Micromachines* **11** 114 (2020)
144. Xin H, Xu R, Li B *Sci. Rep.* **2** 818 (2012)
145. Lee S R et al. *Opt. Express* **18** 25299 (2010)
146. Zhang Y et al. *Opt. Lett.* **43** 2784 (2018)
147. Minz R A et al. *OSA Contin.* **4** 364 (2021)
148. Liu Z L et al. *Opt. Express* **25** 22480 (2017)
149. Gong Y et al. *Opt. Express* **22** 25267 (2014)
150. Zhang C et al. *Micromachines* **10** 499 (2019)
151. Xin H, Li B *Front. Optoelectron.* **12** 97 (2019)
152. Kumar A et al. *J. Phys. Photon.* **2** 025007 (2020)
153. Liu Y, Stief F, Yu M *Opt. Lett.* **38** 721 (2013)
154. Xiang Y et al. *Ann. Physik* **532** 1900497 (2020)
155. Nan F, Yan Z *Adv. Funct. Mater.* **29** 1808258 (2019)
156. Choudhary D et al. *Biomolecules* **9** 26 (2019)
157. Minin I V, Minin O V *Vestn. Sib. Gos. Univ. Geosist. Tekhnol.* **22** 194 (2017)
158. Minin I V et al. *Opt. Express* **28** 22690 (2020)
159. Li Y-C et al. *Light Sci. Appl.* **5** e16176 (2016)
160. Alessandri I, Bontempi N, Depero L E *RSC Adv.* **4** 38152 (2014)
161. Xin H, Li Y, Li B *Adv. Funct. Mater.* **25** 2816 (2015)
162. Xin H, Xu R, Li B *Laser Photon. Rev.* **7** 801 (2013)
163. Li Y et al. *Adv. Funct. Mater.* **29** 1905568 (2019)
164. Wang C et al. *Appl. Phys. Lett.* **109** 011905 (2016)
165. Shvedov V G et al. *Opt. Express* **17** 5743 (2009)
166. Zaltron A et al. *Eur. Phys. J. Plus* **135** 896 (2020)
167. Lyons E R, Sonek G J *Appl. Phys. Lett.* **66** 1584 (1995)
168. Ivanov M et al. *Opt. Express* **25** 1391 (2017)
169. Gong Z et al. *J. Quant. Spectrosc. Radiat. Transf.* **214** 94 (2018)
170. Kalume A et al. *Opt. Lett.* **42** 5113 (2017)
171. Kalume A et al. *Appl. Opt.* **56** 6577 (2017)
172. Kiesel N et al. *Proc. Natl. Acad. Sci. USA* **110** 14180 (2013)
173. Zhang Z et al. *Opt. Express* **20** 16212 (2012)
174. Angelsky O V et al. *Front. Phys.* **8** 114 (2020)
175. Rubinsztein-Dunlop H et al. *J. Opt.* **19** 013001 (2017)
176. Céspedes Vicente O, Caloz C *Optica* **8** 451 (2021)
177. Khonina S N et al. *Micromachines* **11** 997 (2020)
178. Porfirev A P, Skidanov R V *Appl. Opt.* **52** 6230 (2013)
179. Bowman R et al. *Eur. Phys. J. Spec. Top.* **199** 159 (2011)
180. Hashemi Shabestari M et al. *Methods Enzymol.* **582** 85 (2017)
181. Chiou A E et al. *Opt. Commun.* **133** 7 (1997)
182. Priezzhev A, Lee K *Clin. Hemorheol. Microcirc.* **64** 587 (2016)
183. Sparkes I *Curr. Opin. Plant Biol.* **46** 55 (2018)
184. Zhu R et al. *Cells* **9** 545 (2020)
185. Abbondanzieri E A et al. *Nature* **438** 460 (2005)
186. Ritchie D B, Woodside M T *Curr. Opin. Struct. Biol.* **34** 43 (2015)
187. Lee K et al. *J. Biomed. Opt.* **21** 035001 (2016)
188. Constable A et al. *Opt. Lett.* **18** 1867 (1993)
189. Avila R et al. *Opt. Lett.* **42** 1393 (2017)
190. Bowman R W, Padgett M J *Rep. Prog. Phys.* **76** 026401 (2013)
191. Čižmár T et al. *J. Phys. B* **43** 102001 (2010)
192. Asavei T et al. *New J. Phys.* **15** 063016 (2013)
193. Burrow G M, Gaylord T K *Micromachines* **2** 221 (2011)
194. Zemanek P, Karasek V, Sery M *Proc. SPIE* **5514** 15 (2004)
195. Shvedov V G et al. *Opt. Lett.* **37** 1934 (2012)
196. Čižmár T et al. *Phys. Rev. B* **74** 035105 (2006)
197. Shostka N V et al. *Tech. Phys. Lett.* **46** 1107 (2020); *Pis'ma Zh. Tekh. Fiz.* **46** (22) 6 (2020)
198. Redding B et al. *Opt. Express* **23** 3630 (2015)
199. Shostka N et al. *Proc. SPIE* **11525** 1152528 (2020)
200. Hayasaki Y et al. *Opt. Rev.* **6** 24 (1999)
201. Dasgupta R et al. *Appl. Opt.* **50** 1469 (2011)
202. Kirkham G R et al. *Sci. Rep.* **5** 8577 (2015)
203. Burnham D R, McGloin D *Opt. Express* **14** 4176 (2006)
204. Dagalakis N G, LeBrun T, Lippiatt J *Proc. IEEE Conf. Nanotechnol.* 177 (2002)
205. Bhebhe N et al. *Sci. Rep.* **8** 17387 (2018)
206. Gerchberg R W, Saxton W O *Optik* **35** 237 (1972)
207. Liesener J et al. *Opt. Commun.* **185** 77 (2000)
208. Verdeny I et al. *Optica Pura Aplicada* **44** 527 (2011)
209. Bowman R W et al. *Comput. Phys. Commun.* **185** 268 (2014)
210. Pilát Z et al. *J. Photochem. Photobiol. B* **121** 27 (2013)
211. Peña A B et al. *Proc. SPIE* **8427** 84270A (2011)
212. Dienerowitz M, Mazilu M, Dholakia K *SPIE Rev.* **1** 010803 (2010)
213. Erickson D et al. *Lab Chip* **11** 995 (2011)
214. Kawata S, Tani T *Opt. Lett.* **21** 1768 (1996)
215. Anderson P A, Schmidt B S, Lipson M *Opt. Express* **14** 9197 (2006)
216. Yang A H J, Lerdsuchatawanich T, Erickson D *Nano Lett.* **9** 1182 (2009)
217. Yang A H J et al. *Nature* **457** 71 (2009)
218. Lin S, Schonbrun E, Crozier K *Nano Lett.* **10** 2408 (2010)
219. Daly M, Sergides M, Chormaic N *Laser Photon. Rev.* **21** 309 (2015)
220. Luk'yanchuk B S et al. *Opt. Mater. Express* **7** 1820 (2017)
221. Wu M X et al. *Opt. Express* **23** 20096 (2015)
222. Cao Y et al. *Nanomaterials* **9** 186 (2019)
223. Minin I V et al. *Sci. Rep.* **9** 12748 (2019)
224. Han X et al. *Photon. Res.* **6** 981 (2018)
225. Rahmani A, Chaumet P C *Opt. Express* **14** 6353 (2006)
226. Komoto S et al. *ACS Appl. Nano Mater.* **3** 9831 (2020)
227. Jing P et al. *Sci. Rep.* **6** 19924 (2016)
228. Juan M L, Righini M, Quidant R *Nat. Photon.* **5** 349 (2011)
229. Favre-Bulle I A et al. *Nanophotonics* **8** 1023 (2019)
230. Bouloumis T D *Appl. Sci.* **10** 1375 (2020)
231. Kretschmann E, Raether H *Z. Naturforsch. A* **23** 2135 (1968)
232. Bai C et al. *Opt. Express* **28** 21210 (2020)
233. Righini M et al. *Phys. Rev. Lett.* **100** 186804 (2008)
234. Kostina N A et al. *J. Phys. Conf. Ser.* **1461** 012073 (2020)
235. Galloway C M et al. *Nano Lett.* **13** 4299 (2013)
236. Zhang Y et al. *Opt. Express* **25** 32150 (2017)
237. Duhr S, Braun D *Proc. Natl. Acad. Sci. USA* **103** 19678 (2006)
238. Roxworthy B J et al. *Nat. Commun.* **5** 3173 (2014)
239. Garcés-Chávez V et al. *Phys. Rev. B* **73** 085417 (2006)
240. Fang Z et al. *Appl. Phys. Lett.* **94** 063306 (2009)
241. Pin C et al. *ACS Omega* **3** 4878 (2018)
242. Lin L et al. *Acc. Chem. Res.* **51** 1465 (2018)
243. Zhang Y et al. *Light Sci. Appl.* **10** 59 (2021)
244. Liaw J-W et al. *Sci. Rep.* **8** 12673 (2018)
245. Grigorenko A N et al. *Nat. Photon.* **2** 365 (2008)
246. Roxworthy B J et al. *Nano Lett.* **12** 796 (2012)
247. Yoon S J et al. *Nat. Commun.* **9** 2218 (2018)
248. Mestres P et al. *Light Sci. Appl.* **5** e16092 (2016)
249. Koya A N et al. *Adv. Opt. Mater.* **8** 1901481 (2020)
250. Ehtaiba J M, Gordon R *Opt. Express* **26** 9607 (2018)
251. Gordon R *Opt. Laser Technol.* **109** 328 (2019)
252. Horák M et al. *Sci. Rep.* **8** 9640 (2018)
253. Malekian B et al. *Nanoscale Adv.* **1** 4282 (2019)
254. Chen Y et al. *ACS Nano* **10** 11228 (2016)
255. Jiang X et al. *Mater. Lett.* **100** 192 (2013)
256. Manoccio M et al. *Micromachines* **12** 6 (2021)
257. Peterman E J, Gittes F, Schmidt C F *Biophys J.* **84** 1308 (2003)

258. Wang K, Crozier K B *Chem. Phys. Chem.* **13** 2639 (2012)
259. Wang K et al. *Nat. Commun.* **2** 469 (2011)
260. Roxworthy B J, Toussaint K C *Opt. Express* **20** 9591 (2012)
261. Genet C, Ebbesen T W *Nature* **445** 39 (2007)
262. García-Vidal F J et al. *Phys. Rev. B* **74** 153411 (2006)
263. Juan M L et al. *Nat. Phys.* **5** 915 (2009)
264. Neumeier L, Quidant R, Chang D E *New J. Phys.* **17** 123008 (2015)
265. Zheng Y et al. *Nano Lett.* **14** 2971 (2014)
266. Wang G et al. *Opt. Lett.* **41** 528 (2016)
267. Jiang M et al. *Opt. Lett.* **42** 259 (2017)
268. Ma Y et al. *Sci. Rep.* **7** 14611 (2017)
269. Kotsifaki D G, Chormaic S N *Nanophotonics* **8** 1227 (2019)
270. Zhang W et al. *Nano Lett.* **10** 1006 (2010)
271. Roxworthy B J, Toussaint K C *Sci. Rep.* **2** 660 (2012)
272. Roxworthy B J et al. *PLoS One* **9** e93929 (2014)
273. Wan T, Tang B *Nanoscale Res. Lett.* **14** 294 (2019)
274. Korobtsov A V et al. *Quantum Electron.* **44** 1157 (2014); *Kvantovaya Elektron.* **445** 1157 (2014)
275. Shakhov A M et al. *J. Phys. Chem. C* **119** 12562 (2015)
276. Moradi H et al. *Opt. Express* **27** 7266 (2019)
277. Shakhov A, Astafiev A, Nadtochenko V *Opt. Lett.* **43** 1858 (2018)
278. Yan Z et al. *ACS Nano* **7** 8794 (2013)
279. Rykov M A, Skidanov R V *Appl. Opt.* **53** 156 (2014)
280. Porfirev A P, in *Proc. of the Intern. Conf. Inf. Technol. Nanotechnol. Image Processing Systems Institute, Russian Academy of Sciences, Samara, Russia, Samara State Aerospace Univ., Samara, Russia, 2015*, p. 9
281. Berns M W *Front. Bioeng. Biotechnol.* **8** 721 (2020)
282. Xu X, Thomson D J, Yan J *Opt. Express* **28** 33285 (2020)
283. Dienerowitz M et al. *Curr. Microbiol.* **69** 669 (2014)
284. Gong Z, Pan Y, Wang C *Rev. Sci. Instrum.* **87** 103104 (2016)
285. Phillips D B et al. *Nat. Photon.* **8** 400 (2014)
286. MacDonald M P et al. *Opt. Lett.* **26** 863 (2001)
287. Strasser F et al. *Optica* **8** 79 (2021)
288. Xiao K, Grier D G, in *Biomed. Opt. 3-D Imaging* (Washington, DC: OSA, 2010)
289. Būtaitė U G et al. *Nat. Commun.* **10** 1215 (2019)
290. Whyte G et al. *Opt. Express* **14** 12497 (2006)
291. Sinjab F et al. *Opt. Express* **26** 25211 (2018)
292. Onda K, Arai F, in *2012 IEEE Intern. Conf. Robot. Autom.* (Piscataway, NJ: IEEE, 2012) p. 1069
293. Ploschner M et al. *Nano Lett.* **12** 1923 (2012)
294. Kotsifaki D G, Makropoulou M, Searfetinides A A *EPJ Appl. Phys.* **86** 30501 (2019)
295. Vossen D L J et al. *Rev. Sci. Instrum.* **75** 2960 (2004)
296. Svoboda K, Yasuda R *Neuron* **50** 823 (2006)
297. Moradi A-R et al. *Three-Dimensional Imaging, Vis. Disp. 2011* **8043** 804310 (2011)
298. David G et al. *Commun. Chem.* **1** 46 (2018)
299. Shostka N V et al. *J. Phys. Conf. Ser.* **1410** 012162 (2019)
300. Castaño G et al. *Molecules* **12** 3325 (2019)
301. Plöschner M et al. *Sci. Rep.* **5** 18050 (2016)
302. Yang Z et al. *Biomed. Opt. Express* **6** 2778 (2015)
303. Otto O et al. *Opt. Express* **18** 22722 (2010)
304. Keen S et al. *J. Opt. A* **9** S264 (2007)
305. Neuman K C, Block S M *Rev. Sci. Instrum.* **75** 2787 (2004)
306. Cheezum M K, Walker W F, Guilford W H *Biophys. J.* **81** 2378 (2001)
307. Dholakia K, Čižmár T *Nat. Photon.* **5** 335 (2011)
308. Mosk A P et al. *Nat. Photon.* **6** 283 (2012)
309. Staunton J R et al. *Opt. Express* **25** 1746 (2017)
310. Nicholas M P, Rao L, Gennerich A, in *Methods in Molecular Biology* (Ed. D J Sharp) (New York: Springer, 2014)
311. Flusberg B A et al. *Nat. Meth.* **2** 941 (2005)
312. Hanstorp D et al. *Proc. SPIE* **10347** 103472C (2017)
313. Gong Z et al. *Anal. Chim. Acta* **1020** 86 (2018)
314. Jordan P et al. *Lab Chip* **5** 1224 (2005)
315. Girkin J M, Carvalho M T *J. Opt.* **20** 053002 (2018)
316. Honda K et al. *Nature* **434** 772 (2005)
317. Curran A et al. *Optica* **1** 223 (2014)
318. Botcherby E J et al. *Opt. Commun.* **281** 880 (2008)
319. Kemper B et al. *J. Biophotonics* **3** 425 (2010)
320. Cheong F C, Krishnatreya B J, Grier D G *Opt. Express* **18** 13563 (2010)
321. Pitkäaho T, Manninen A, Naughton T J *Appl. Opt.* **58** A202 (2019)
322. Rivenson Y, Wu Y, Ozcan A *Light Sci. Appl.* **8** 85 (2019)
323. Shostka N V et al. *J. Phys. Conf. Ser.* **1697** 012161 (2020)
324. Berg M J, Videen G *J. Quant. Spectrosc. Radiat. Transf.* **112** 1776 (2011)
325. Bzdek B R et al. *J. Chem. Phys.* **145** 054502 (2016)
326. Kemppinen O et al. *Sci. Rep.* **10** 16085 (2020)
327. Simon B et al. *Optica* **4** 460 (2017)
328. Hsu W-C et al. *Opt. Lett.* **39** 2210 (2014)
329. Vishnyakov G N et al. *Opt. Spectrosc.* **121** 947 (2016); *Opt. Spektrosk.* **121** 1020 (2016)
330. Kim K et al. *Opt. Express* **21** 32269 (2013)
331. Zhang T et al. *Phys. Rev. Lett.* **111** 243904 (2013)
332. Lin Y et al. *Opt. Lett.* **42** 1321 (2017)
333. Wang M D et al. *Biophys. J.* **72** 1335 (1997)
334. Lúcio A D, Santos R A S, Mesquita O N *Phys. Rev. E* **68** 041906 (2003)
335. Singh G P et al. *Anal. Chem.* **77** 2564 (2005)
336. Xie C et al. *Anal. Chem.* **77** 4390 (2005)
337. Zheng F, Qin Y, Chen K *J. Biomed. Opt.* **12** 034002 (2007)
338. Chan S-A et al. *Talanta* **69** 952 (2006)
339. Collard L, Sinjab F, Notingher I *Biophys. J.* **117** 1589 (2019)
340. Townes-Anderson E et al. *Mol. Vis.* **4** 12 (1998)
341. Yadav A et al. *Phys. Rev. E* **101** 062402 (2020)
342. Buican T N et al. *Appl. Opt.* **26** 5311 (1987)
343. Lee K S et al. *Nat. Protoc.* **16** 634 (2021)
344. Wang M M et al. *Nat. Biotechnol.* **23** 83 (2005)
345. MacDonald M P et al. *J. Biol. Regul. Homeost. Agents* **18** 200 (2004)
346. Ozkan M et al. *Langmuir* **19** 1532 (2003)
347. Bahadori A, Oddershede L B, Bendix P M *Nano Res.* **10** 2034 (2017)
348. Bolognesi G et al. *Nat. Commun.* **9** 1882 (2018)
349. Liang H et al. *Biophys. J.* **70** 1529 (1996)
350. Neuman K C et al. *Biophys. J.* **77** 2856 (1999)
351. Wang C et al. *J. Biomed. Opt.* **18** 045001 (2013)
352. König K et al. *Cell. Mol. Biol.* **42** 501 (1996)
353. Leitz G et al. *Biophys. J.* **82** 2224 (2002)
354. Liu R et al. *Exp. Hematol.* **41** 656 (2013)
355. Ng K S, Zhou Z L, Ngan A H W *J. Cell. Physiol.* **228** 2037 (2013)
356. Dasgupta R et al. *J. Biomed. Opt.* **15** 055009 (2010)
357. Im K-B et al. *J. Korean Phys. Soc.* **48** 968 (2006)
358. Ayano S et al. *Biochem. Biophys. Res. Commun.* **350** 678 (2006)
359. Landry M P et al. *Biophys. J.* **97** 2128 (2009)
360. Aabo T et al. *J. Biomed. Opt.* **15** 041505 (2010)
361. Pilát Z et al. *Sensors* **17** 2640 (2017)
362. Liu Y et al. *Opt. Lett.* **20** 2246 (1995)
363. Anquez F et al. *Photochem. Photobiol.* **88** 167 (2012)
364. Sokolovski S G et al. *Sci. Rep.* **3** 3484 (2013)
365. de With A, Greulich K O *J. Photochem. Photobiol. B* **30** 71 (1995)
366. Mohanty S K et al. *Radiat. Res.* **157** 378 (2002)
367. Walter J et al. *J. Microsc.* **209** 71 (2003)
368. Kong X et al. *Nucleic Acids Res.* **37** e68 (2009)
369. Wang Y et al. *Appl. Phys. Lett.* **105** 173703 (2014)
370. Vorobjev I A et al. *Biophys. J.* **64** 533 (1993)
371. Bregnhøj M et al. *J. Phys. Chem. B* **119** 5422 (2015)
372. Liang H et al. *Lasers Surg. Med.* **21** 159 (1997)
373. Palima D et al., in *Photonics*: *Biomedical Photonics, Spectroscopy, and Microscopy, IV* (Ed. D L Andrews) (New York: John Wiley and Sons, 2015) Ch. 6, https://doi.org/10.1002/9781119011804.ch6
374. Zhang Z, Milstein J N *BioRxiv* 808352 (2019)
375. Arbore C et al. *Biophys. Rev.* **11** 765 (2019)
376. Blázquez-Castro A *Micromachines* **10** 507 (2019)
377. Korobtsov A et al. *Laser Phys.* **22** 1265 (2012)
378. Huang Y-X et al. *Biomed. Opt. Express* **9** 1783 (2018)
379. Baudoin M et al. *Nat. Commun.* **11** 4244 (2020)
380. Lo W-C et al. *Proc. Natl. Acad. Sci. USA* **118** e2023188118 (2021)